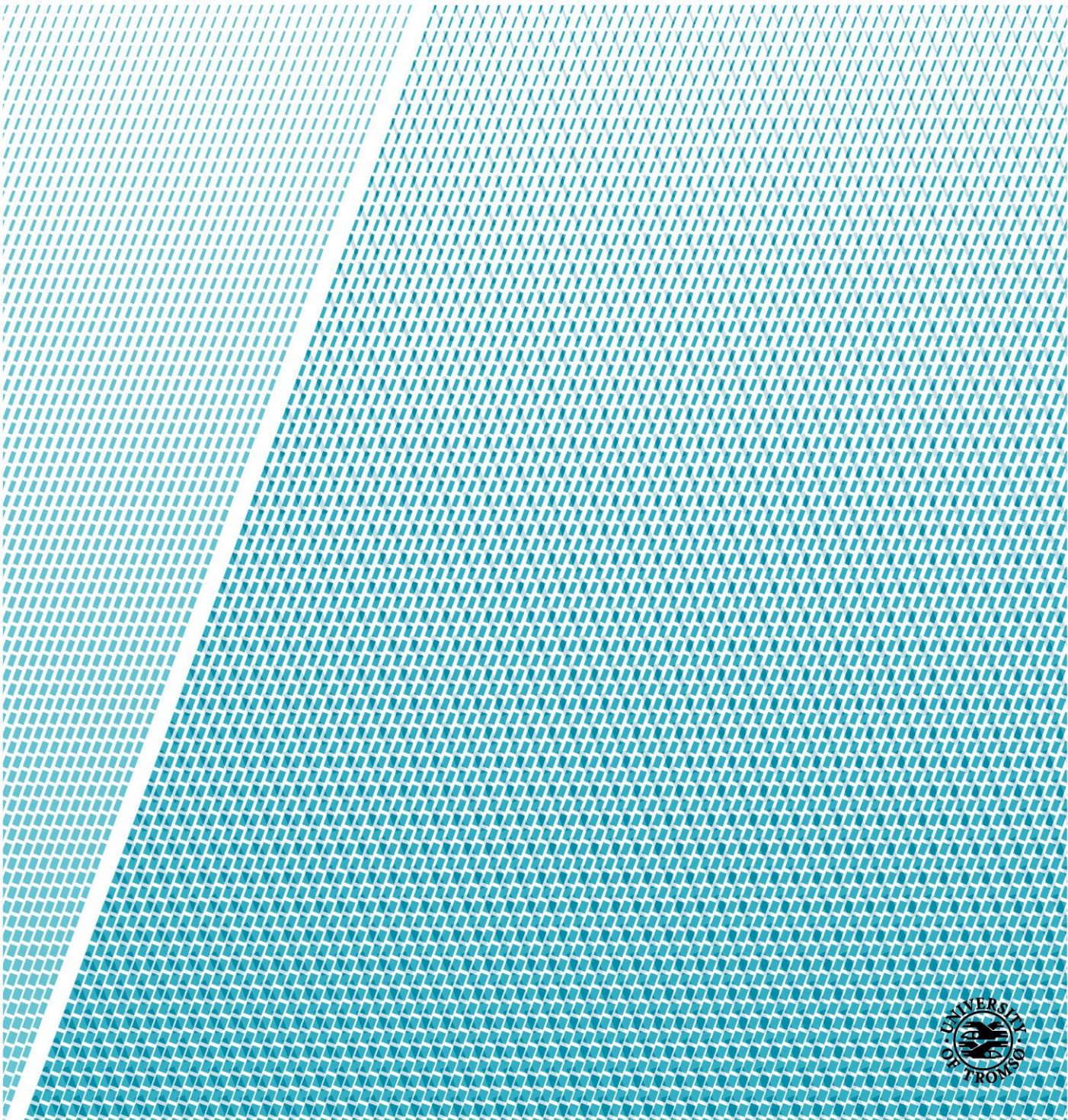


Wireless Charging for Small Electric Vessels

Hafeez Abolade Omosanya

Master's thesis in Electrical Engineering ... June 2019



ABSTRACT

With the presence of traditional thick and heavy cables for charging, the risk of humans exposed to high-voltage, and due to mechanical wear and tear in conductive materials, inductive wireless charging was introduced which is the future of charging technology. This project has focused on magnetic-coupled wireless transfer with some key components involved such as a DC voltage source, a full-bridge inverter, LLC resonant tank, an isolated transformer, a full-bridge rectifier, and a resistance load. Various topologies were consulted from previous literatures on Electric Vehicles, buses, and trams but only one topology was adopted, which is the LLC resonant converter topology. A successful wireless transfer of energy was made after careful modelling and simulation, design and construction were done with desired specifications. A laboratory prototype was also built and the design steps, its theoretical analysis, and required calculations can be seen in this report. This project will serve as a guide for small electric vessels in choosing and implementing the optimum wireless charger at a beneficial cost.

Keywords: *wireless power transfer, inductive power transfer, operating or switching frequency, resonant frequency, inductive coils, LLC resonant converter*

ACKNOWLEDGEMENT

My profound gratitude goes to God almighty for his protection and guidance throughout my course of study. I will also say a big thank you to Parents, my brothers especially Dr. Kamaldeen and Dr. Kabir, Mr. Monsur and Mr. Surajdeen, for the support throughout my entire life and for their well wishes.

I would also like to show my sincere gratitude to my supervisor: Associate Professor Bjarte Hoff for his guidance, support, patience, motivation, assistance and technical guidance throughout the duration of this work.

I will end this section by showing my gratitude to my course mates especially Hussein and Maya for always pushing me to give it my best, and house mates. Thank you very much for the love and care.

Table of Contents

ABSTRACT	i
ACKNOWLEDGEMENT	ii
1 INTRODUCTION.....	1
1.1 GMV Zero	2
1.2 Project Description	4
1.2.1 Problem Analysis	4
1.2.2 Project Limitation.....	4
1.2.3 Project formulation/objectives	5
1.3 Thesis Structure and Layout.....	6
1.4 Resources.....	7
1.4.1 Software	7
1.4.2 Hardware	7
2 LITERATURE REVIEW.....	8
2.1 Wireless Power Transfer methods and different Topologies	9
3 METHODOLOGY	15
3.1 Converter Voltage Gain.....	17
3.2 Modes of Operation	19
3.2.1 Switching/operating frequency is equal the resonant frequency $f_s = f_r$	22
3.2.2 Switching frequency is greater than the resonant frequency $f_s > f_r$	22
3.2.3 Switching frequency is less than the resonant frequency $f_s < f_r$	23
3.3 Design Steps	23
3.3.1 STEP 1: Selecting the Q_{max} Value.....	24
3.3.2 STEP 2: Selecting m value	25
3.3.3 STEP 3: Finding the Least Normalized Switching Frequency	26
3.3.4 STEP 4: Voltage Gain Verification (K)	27

3.3.5	STEP 5: Calculating Resonant Components Values.....	27
3.4	Full-Bridge Inverter, Resonant tank and Full-bridge Rectifier Selection	28
3.4.1	Full-Bridge Inverter.....	28
3.4.2	Resonant Tank.....	31
3.4.3	Full-Bridge Rectifier	31
3.5	Design Example and Calculation	33
3.5.1	Application and Specifications.....	33
3.5.2	Design Steps	33
3.6	Laboratory Setup Description.....	36
4	Coil Design.....	38
4.1	Theoretical Analysis	38
4.2	LITZ wire	39
4.2.1	Choosing number and diameter of strands.....	40
4.2.2	Choosing construction.....	43
4.3	Technical Basics and Calculation.....	43
4.3.1	Right-hand-rule	43
4.3.2	How to calculate the number of turns in the primary coil.....	44
4.3.3	Skin-effect and skin depth.....	44
4.3.4	Relationship of single wire diameter to range of frequency	46
5	CHALLENGES.....	49
6	RESULTS AND ANALYSIS	50
6.1	Hardware (Small Application).....	55
7	CONCLUSION	57
7.1	Future works	57
	REFERENCE.....	58

List of Tables

Table 3.1: the comparison between high and low m value	26
Table 3.2: the target specification for the heavy load and light load	33
Table 4.1: the parameters for economical Litz-wire designs [27].....	42
Table 4.2: parameters for skin depth of copper Litz wire with frequency [25]	45
Table 4.3: the relationship between recommended single wire diameter and frequency range [25]	46
Table 4.4: System specifications	47
Table 4.5: design parameters for the transmitting and receiving coils I designed	47
Table 6.1: the target specification for the resonant converter	51
Table 6.2: simulation and hardware results.....	52

List of Figures

Figure 1.1: the GMV ZERO electric vessel	3
Figure 1.2: the thesis structure and layout.....	6
Figure 2.1: the topology used in [10]	10
Figure 2.2: a block diagram of the Dynamic Wireless Charging (DWC) described in [14]....	11
Figure 2.3: the three coil arrangements described in [15].....	11
Figure 2.4: an illustration of the topology described in [17].....	12
Figure 2.5: the CLLLC topology described in [16]	13
Figure 2.6: the equivalent circuit of the dual-coupled robust WPT system described in [11].	14
Figure 3.1: a block diagram of the Wireless Charger	15
Figure 3.2: a full bridge LLC converter circuit with a boost converter in the secondary side.	16
Figure 3.3: the equivalent resonant circuit	17
Figure 3.4: the gain curves [29]	19
Figure 3.5: the converter's three modes of operation [29]	20
Figure 3.6: first half of switching cycle in positive direction [29].....	21
Figure 3.7: second half of switching cycle with negative voltage and direction [29].....	21
Figure 3.8: first half of freewheeling [29].....	22
Figure 3.9: second half of freewheeling [29]	22
Figure 3.10: design flow chart.....	24
Figure 3.11: the voltage gain plot with different values of Q [29].....	25
Figure 3.12: the same resonant tank gain plots but different m values [29]	26

Figure 3.13: the half bridge and full bridge inverter circuit.....	29
Figure 3.14: my Inverter Circuit with its resonant tank which I designed using MATLAB&SIMULINK	29
Figure 3.15: the Drives board from University of Minnesota for the Inverter Circuit (primary side).....	30
Figure 3.16: the positive and negative half cycle of a full-bridge rectifier	32
Figure 3.17: my full-bridge rectifier	33
Figure 3.18: the gain plot [29].....	35
Figure 3.19: the whole laboratory setup.....	37
Figure 4.1: the diameter of a standard Litz wire [25].....	39
Figure 4.2: a typical unserved basic Litz Wire [25].....	40
Figure 4.3: the flowchart of the Litz Wire design steps	40
Figure 4.4: Examples of how the winding breadth b and the number of turns per section are defined for some common winding geometries. [19, 27]	41
Figure 4.5: the magnetic field (H) and current flow in the inductor, and skin depth.....	45
Figure 4.6: the transmitter (Tx) and receiver (Rx) Litz-wire coil I constructed	48
Figure 6.1: the simulation circuit for the wireless charger.....	50
Figure 6.2: the hardware laboratory setup corresponding to the circuit above	51
Figure 6.3: the 400vDC_Inverter Voltage and Current waveform at full load at 50% Duty Cycle.....	52
Figure 6.4: Output voltage of the 400 v DC source at no load is (627 V)	53
Figure 6.5: the waveform at full-load voltage (322 v DC) and current (2.5 A).....	53
Figure 6.6: the 12v DC Inverter Voltage and Current waveform at full load (closed circuit) at 50% Duty Cycle	54
Figure 6.7: 12vDC_Transformer input and Output V&I waveform at full load (closed circuit) at 75% duty cycle	54
Figure 6.8: 12v DC Output Voltage at no load (open circuit) (10.1 V).....	55
Figure 6.9: output waveform for 12 v DC at full-load (6.975 ohms), (7.26V), (1.04 A).....	55
Figure 6.10: the output voltage of the laboratory setup	56
Figure 6.11: the waveforms of the output voltage and current of the inverter.....	56

Acronyms

FETs - Field Effect Transistors
ZVS - Zero Voltage Switching
ZCS - Zero Current Switching
MOSFET - Metal Oxide Field Effect Transistors
IGBT - Insulated Gate Bipolar Transistor
PWM - Pulse Width Modulation
DCM - Discontinuous Conduction mode
CCM - Continuous Conduction Mode
VSI - Voltage Source Inverter
CSI - Current Source Inverter
DC - Direct Current
AC - Alternating Current
EMI - Electromagnetic interference
WPT - Wireless Power Transfer
PIV – Peak Inverse Voltage
IPT - Inductive Power Transfer
ICPT - Inductively Coupled Power Transfer
SQW - Square Wave
PSW - Pure Sine Wave
MCU - Microcontrollers
DWC - Dynamic Wireless Charging
EV - Electric Vehicle
QWC - Quasi-Dynamic Wireless Charging
SWC - Static Wireless Charging
FEM - Finite Elements Method

1 INTRODUCTION

The world is changing so fast, and what looked like a fantasy is becoming our reality. It seems that progress spreads to all spheres of humanity's life, but one of the most amazing breakthroughs has been achieved in energy. About two decades ago, it appeared there was no effective alternative to the conventional fossil fuels such as gasoline and oil, but it turned out that there is a better, cleaner, and more effective substitute to them: electricity.

The maintenance cost of electric vessels is lower than the one of those fuelled by conventional diesel. Fuel prices heavily depend on the political and military situation in countries providing oil; even if we do not take it into consideration, one year of running a conventional vessel would cost you thousands/millions of Norwegian Kroner. At the same time, running an electric maritime vessel would cost you significantly less in a year.

“The practical importance of the wireless power transfer (WPT) systems has been obvious since the time of N. Tesla, and recent advances in this field, accompanied by the exponential growth in the request for fast and efficient wireless charging of battery-powered devices, has made these systems especially topical” [12]. The two main categories of wireless power transfer (WPT): magnetic-coupled power transfer and electric-coupled power transfer. Up till date, many real-world applications use the magnetic-coupled power transfer technology to achieve wireless charging. For example,

Implantable medical devices, portable equipment, e-bike, plug-in hybrid vessels, electric vehicles and so on. The electric-coupled power transfer technology is used in dynamic devices and instances which are restricted by space, such as synchronous machines and internal isolations [11]. Moreover, IEEE Xplore Digital Library website has published more than 7500 articles on wireless power transfer which are available to the public. Within the years 2014 to 2017, the researchers have published more than 5,000 articles based on previous articles [13].

In [14], an advantage of wireless charging can be said to be its safety and convenience of charging while the part being charged is at rest. Research and development have been focused mainly on cost and efficiency because inductive power transfer which is adopted for wireless charging is a lead technology for the widespread presence of electric vessels [15]. The

technical challenges that are related to wireless charging infrastructures includes its modelling, simulation, design, construction, operation, and maintenance of the infrastructure. There are lots of wireless charging development stages that are involved when using the magnetic coupler, and it has some of the properties of a transformer with few millimetres distance between the transmitter (Tx) which is the primary coil and the receiver (Rx) also known as the secondary coil [14]. Another fundamental challenge of inductive power transfer (IPT) systems is to increase the positioning tolerance between transmitter and receiver coils and to ensure the interoperability for a variety of vessels [16]. It is said that the power that can be transferred and the efficiency in IPT systems to a great degree depend on a coupling factor called k , which diminishes with an increasing air gap to coil size ratio. With respect to power electronics, the design alongside the fundamental function and operation of a series compensated resonant converter is discussed in this paper but it is not the main objective of this project [17].

In [10], the Inductively Coupled Power Transfer (ICPT) system makes it feasible to charge wirelessly at a range of distance to prevent safety matters and to provide comfort to the users. Although the ICPT system has been successful for the charging of the electric vehicles, but it continues to have some challenges, prominently limitation of misalignment tolerance and low efficiency of the overall circuit.

1.1 GMV Zero

When trying to farm fish sustainably, it makes sense to tend the farm with a supply vessel that is also environmentally friendly. GMV Zero is a workboat designed for daily tending of fish farms. GMV Zero is the world's first fully-electric boat. The boat is to be used by Trollvika operation, owned by Northern Light Salmon and Sørrollnes Fisk [2].

The pilot house is equipped with a pantry and seating area designed for about 4 persons. The main deck is fitted with a wardrobe, a work or washbasin, and a separate toilet room. The vessel will have a cruise ship of more than 10 knots and a range of over 26 nautical miles at 8 knots. This boat will save the environment from emissions of approximately 900 kg of NO_x (nitrogen oxide) and 90 tonnes of CO₂ (carbon dioxide) annually and will also save 200,000 kroner in annual fuel costs compared to a traditional diesel boat. GMV Zero has its main dimensions 13.97 x 7.6 x 2.40 meters, and has an on-board crane certified for 32 tonne-meters lifting. With two capstans of 3 tonnes and hydraulic HP-washer, the vessel is ready for a wide

range of operations during fish farm tending. Two electrical main propulsion motors of 107 kW together with an electric bow thruster gives impeccable response while manoeuvring [2].



Figure 1.1: the GMV ZERO electric vessel

1.2 Project Description

1.2.1 Problem Analysis

The problem is that there are no quick chargers with enough power and low enough weight to be mounted on board for the fish farm electric vessel. Also, in general, when it comes to charging of GMV Zero, the main concern is the thick and heavy cable that the crew needs to plug in every day to charge the boat. Docking time is much longer than that of a ferry, since the boat mainly will charge over-night in addition to lunch breaks, if required. Wireless charging could make the whole procedure easier and at the same time, reduce the wear and tear that will occur with cables and plugs.

Introducing the inductive charging power transfer technology to the marine sector initiates certain challenges. The most obvious one is that electric fishing boats require outstanding higher energy and power levels for operating between two charging ports i.e. the receiving end and the sending end, as compared to city buses, trams, and some electric vehicles. The inductive charger as a result of that must be able to deliver power in several hundred-kilowatt power range, by preference in a single unit. Besides, for point-based high-power battery charging, road or rail vehicles are normally immobilized while charging. By contrast, a docked vessel can move with respect to the fixed onshore charging structure during charging operation due to the combined action of the wind, waves, and draft of the vessel, also in reaction to the change in tilt and draft that results from loading and unloading the vessel. The charging system must be designed so that the amount of power transferred, as well as efficiency and safety in operation, are not compromised despite such movements. This means that the system should have a high tolerance to misalignment and variations in airgap distance and that it should be controlled to automatically compensate for the effect of such differences in relative position [1].

1.2.2 Project Limitation

There are two major types of wireless power transfer but in this project, I will focus and will work using the magnetic-coupled power transfer also known as the inductive coupling.

In addition to that, there are several topologies that can be used in the resonant converter namely L filter, LC filter, LCL filter, LCCL filter, CLLC filter and so on but I will be using the high-order LLC filter because the time allocated to this project is quite limited and the

LLC filter seems to be the best topology for this case in order to get the best of results and also provide attenuation for the PWM carrier and side-band voltage harmonics.

In [13], it is suggested the square wave (SQW) inverter topology be used as compared with the pure sine wave (PSW) simply because it may be a better option in the sense that the design of the SQW is simpler, it has a lower loss, lower switching frequency, fewer components, low manufacturing cost, and shorter microcontrollers (MCU).

The GMV Zero type vessel which I am proposing a solution to in this project has 350KWh battery power and 2 electrical main proportion motors of 107KW. When these motors are being used, from basic calculations, the battery would last for approximately 3.3 hours. But with other electrical appliances onboard, I'll assume it lasts for 3 hours. So therefore, I need to simulation and design a wireless charger that would charge a 350KWh battery and not more that rated power of the battery.

1.2.3 Project formulation/objectives

1.2.3.1 Formulation

The goal of the project is to model and simulate, design and construct a wireless charging system for small electric vessels.

1.2.3.2 Objectives

The main objectives of this project are as follows:

1. Overview of existing wireless charging solutions, with focus on inductive charging.
2. Evaluate and propose a solution for charging a GMV Zero type vessel from other areas such as electric cars and large ferries or ships.
3. Modelling and simulation of a selected wireless charging solution, with focus on the power electronics and control systems.
4. Design a prototype laboratory setup for wireless charging.
5. Construct a prototype and perform small scale experiment (if time permits).

1.3 Thesis Structure and Layout

This project is structured as follows: In the first chapter, an introduction is made to the research topic and motivated. The second chapter introduces the reader to some common wireless charging topologies and operations, discusses some technologies that are currently driving the maritime vessels and electric vehicles. In chapter three, a full-bridge LLC converter was simulated and modelled, designed and constructed according to desired specification, and a description of the laboratory setup. You will also find the design steps in chapter three. Chapter four discusses the inductive coil design, its basic calculations and how to select the optimal coil. In chapter five, some challenges were highlighted. Chapter six discusses the results and analyses. Chapter seven is the final chapter of this work, and it presents the conclusions. In this chapter, a reflection is given on the work done and possibilities for future work is proposed.



Figure 1.2: the thesis structure and layout

1.4 Resources

1.4.1 Software

MATLAB/Simulink software and dSPACE control desk will be used to do the modelling and simulation of this project.

1.4.2 Hardware

Below is a list of some of the hardware that will be used in this project:

1. Inverter.
2. Inductive Coupler.
3. Rectifier.
4. Capacitor.
5. Inductor.
6. MOSFETS.
7. Diodes.
8. Battery.
9. Oscilloscope.
10. Transformer.
11. DC Power Supply.
12. Functions generator.
13. Variable resistor.

2 LITERATURE REVIEW

By making practical and effective use of free electrons in a conducting material, electrical energy has been able to move from one place to the other. Current can flow in this conducting material when the potential difference is put to practical use across the conducting material, and as a result of this, electric power can be fetched from a battery or a generator or other types of power source.

The traditional way of transferring energy from different power sources to the load is by using wires and cables be it in our homes, industries, and other places, and the choice is easy since the load in these places are stationary or motionless. However, due to technology advancements, electrical products are becoming smarter and hence relying on cables to be connected to a power outlet is becoming archaic, stressful, and less relevant. Also, in some cases, it may be dangerous to have cable connections because of high voltage exposure, electric shocks and sparks.

Research and development of hybrid and electrical vehicles is rapid and fast growing because of the increase in oil prices and due to the concerns of the public and the negative effect fossil fuels have on the environment. Hybrid and electrical vehicles have an on-board battery connected to them which can make available partial power or full electric power for transportation of an entire journey. These batteries are basically charged using cable connections but there are more options being explored if they are charged wirelessly or without the use of cables. The batteries could be charged while moving or while parking to order pizza or something. More of the options explored with wireless charging is that cost of maintenance is very reduced and no problem of wear and tear since it is contactless.

In WPT, electrical energy is converted to another form of energy which can be transferred by using inductive coils without the need of connecting conductive wires. A common and simple example of transferring energy wirelessly can be seen in our radios at home, in our offices or in the car, where radio waves transfer information such as sound, video and data. As wireless transfer of energy or wireless power transfer appears to be an alternative or better way of charging our products, it still has many design setbacks and technological improvements which needs to be tackled. [31]

2.1 Wireless Power Transfer methods and different Topologies

MOBIMAR (Mobile Marine Applications), Growth in the amount of full electric and hybrid vessels have brought up the importance of fast charging in addition to the rapid charging connection after vessel mooring. Extra weight and cost of batteries onboard must be minimized as well as the mooring time. Due to this, either current or voltage, must be in high level to keep the charging effective i.e. optimized time wise. In alternating current (AC) systems the voltage is extremely high over the charging connection whereas in direct current (DC) systems the current is high. DC can also have high voltage as well, but it depends on the application with which you are using it and the solution required for the problem. Difference between AC/DC charging connectors is if the quay or ship side needs to be simple and light. In AC-systems the quayside can be built simple and cheap. DC-systems are more cost-effective and lighter for the ships. Criteria of evaluation can depend on how many ports vessel must visit, which are the grid limits onshore, does the vessel size or speed allow carrying weight from transformers, rectifiers and chargers on-board. Current efficiency of electric ferries suffers technically about the complexity of establishing the charging connection systems nearshore. Above all, the economical competitiveness of the electrification is lost with massive seabed constructions. These seabed foundations are essential for many feeding connectors and precise mooring systems operating from the shipside some 20-50 meters offshore depending on the ship length [5].

Kafeel Ahmed Kalwara, Muhammad Aamir, and Saad Mekhilef; proposed a design procedure which optimizes the electrical parameters involved in the Inductively Coupled Power Transfer (ICPT) system and match them up with geometrical dimensions of the charging coils involved in the charging of electric vehicles. The methodology presented in their paper helps in choosing suitable and proper dimension of the coils and electrical parameters to manage with the issue of misalignment tolerance. A program based on the mathematical model was developed in MATLAB software to determine optimal values of overall ICPT system circuit parameters and the geometrical dimensions of coils. The experiments of the ICPT system have been carried out with developed optimal coil design for 1 kW power transfer at various air gaps. The misalignment tolerance of the ICPT system was recorded and presented in their paper. Their proposed optimal design achieves maximum efficiency of 90.5% at perfect alignment, however, it maintains the efficiency of 72% at 35–40% misalignment between the coils. The misalignment test results support the design of coils for EV charging application.

Generally, there are a few studies that have been conducted for complete design optimization of ICPT system. The optimization should include optimized number of turns of coils, their cross section for any desired level of power. [10].

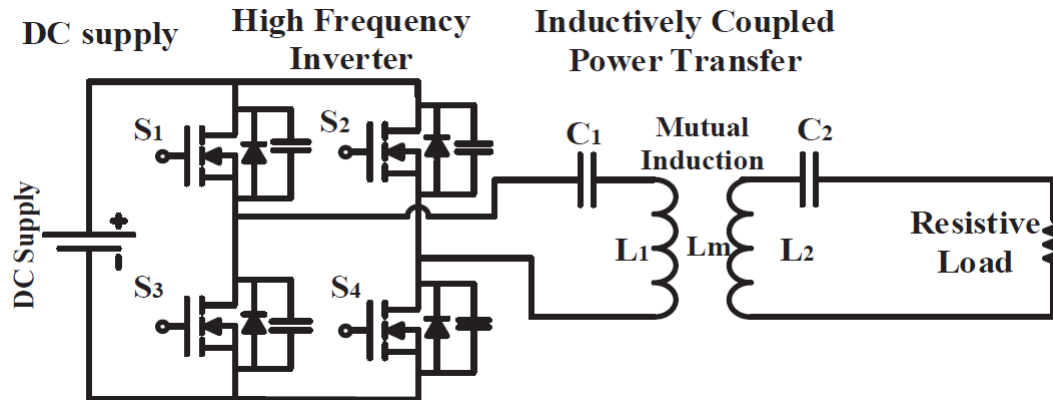


Figure 2.1: the topology used in [10]

In [14], *Aqueel et al* in their publication talked about the different wireless charging technologies and their implementation. They started with the Static Wireless Charging (SWC) which due to the enhanced alignment produces a more effective efficiency in power transfer with different stages involved, and each stage with its complexity and efficiency. Secondly, they discussed about the Dynamic Wireless Charging (DWC) which eliminates the need to stop and charge of an EV. This technology charges your vehicle while in motion and it is expensive to implement because of the need to install an existing magnetic coupler under the road surface supplied with a high-frequency current generating electromagnetic field, and a pickup coil installed in the EV. “DWC overcomes most of the problems of the EV, such as range anxiety, battery size, and battery cost”. And lastly, they discussed about Quasi-Dynamic Wireless Charging (QWC) which I call the hybrid implementation which allows the charging possibility while moving slowly or in a stop and move situation. For example, in a traffic situation. This is basically done by designing an auto-detection system for charging in this condition which automatically detects whether you are driving or in a stationary position and switches between the SWC and the DWC effortlessly. This implementation of the QWC would have been very relevant and useful for this project as stated in section 1.2.1, discussing the problem analysis about how the vessel is disoriented due to the combined action of wind, waves, tilt and draft that result from loading and unloading the vessel.

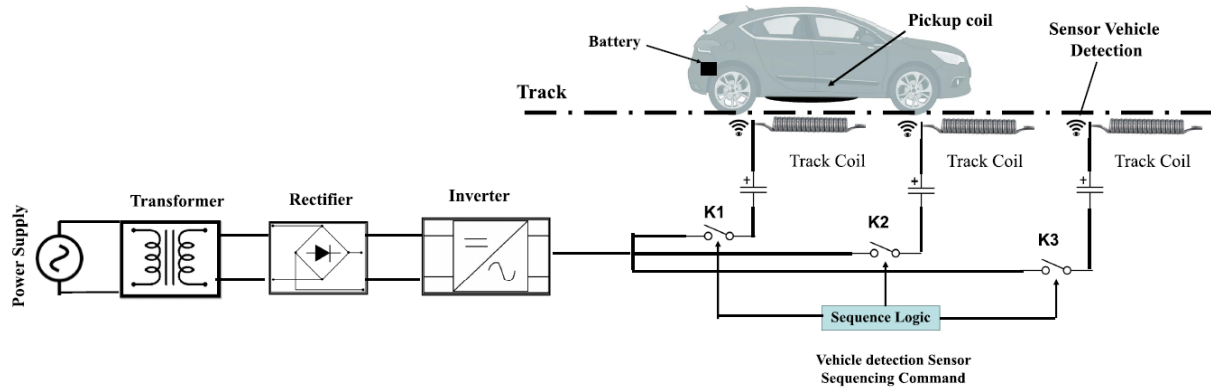


Figure 2.2: a block diagram of the Dynamic Wireless Charging (DWC) described in [14]

In [15], *Fraunhofer* wrote about the minimization of the air gap between the primary/sending side (charging station) and the secondary/receiving side (pick-up coil) which is a feasible way of achieving an increase in efficiency and a way to reduce the external stray fields. This brochure also introduced three coil arrangements capable of achieving a reduction in system costs and required positioning tolerance which are: Non-adaptive – highly tolerant, Non-adaptive – medium tolerant, and Adaptive Primary Coil.

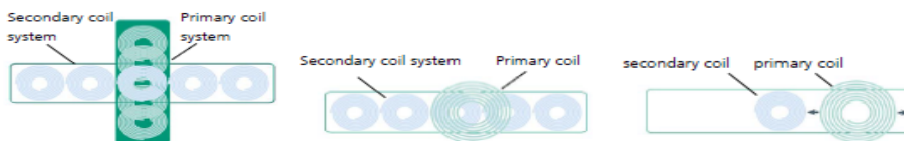


Figure 2.3: the three coil arrangements described in [15]

In [17] *Christopher et al.*, in their paper proposed a concept and focused their objective on minimizing the air gap between transmitter (primary) and receiver (secondary) coils with respect to an autonomous parking method with a feasibility of values smaller than 20mm. Therefore, a design and optimization process were performed but it is very principal to set out the mechanical and electrical constraints for the magnetic design of the multi-coil system for the inductive power transfer (IPT) for charging electric vehicles. This will help in decreasing cost of material and minimizes the external stray fields as compared to systems with large air gaps. Soon after the installation space and anticipated air gap have been defined, a coil geometry was chosen on the underlying support or foundation of finite elements method (FEM) simulation. Later the achievable coupling factor and realization of the required inductance is carried out, which led them to the investigation of the frequency dependent winding losses by two different numeric approaches. In the end, these design features or

properties were considered in order to build up a prototype system to match with the results from the simulation. Their IPT system consists of one primary and a set of five secondary circular coils with an outer coil radius of 55 mm and the secondary coils are aligned in a single pick-up housing. They achieved an efficiency between 92% and 96% at an output power of up to 3.5 kW as a result.

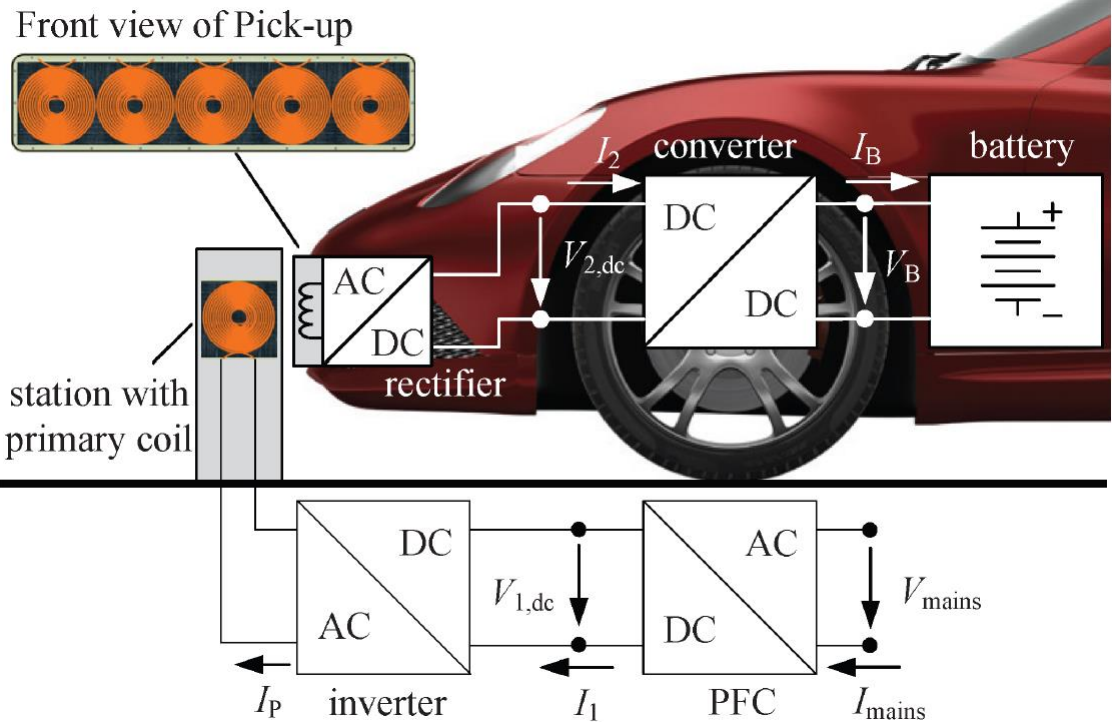


Figure 2.4: an illustration of the topology described in [17]

Molly Lempriere of Power Technology, A research team at Stanford University has hit a breakthrough in its work on developing wireless power transfer. The project is focused on the transfer of power for moving objects, building on previous work undertaken at Massachusetts Institute of Technology into transmitting power over a few feet for stationary objects.

In June 2018, the researchers, led by professor of electrical engineering Shanhui Fan, published a study entitled *robust wireless power transfer using a nonlinear parity-time-symmetric circuit*, explaining how they have effectively managed to transfer small amounts of power between moving objects. This is a significant breakthrough for the technology, bringing it closer to real-life application [7].

Christopher *et al* in [16], presented in their paper, a novel positioning tolerant inductive power transfer (IPT) and because of its special structure, the system allows for necessary interoperation between different vehicles. Besides, additional publications have tested and proven that the coupling factor k is conditional to the vertical and horizontal distance between the transmitter (primary) and the receiver (secondary) coils of the IPT system. An orthogonal alignment between the primary and secondary coil system presents some tolerance with higher position. They also researched in their paper, different coil shapes in order to attain maximum coupling in the case of air gap and misalignments because the inductive power transfer depends on the magnetic coupling and coil attributes. Due to this investigation, a special orthogonal coil arrangement and system was designed. They showed some FEM-simulations and measurements, and they were able to achieve their design of an IPT which is position tolerant and allows interoperation between a large variety of car models using a bidirectional resonant converter (CLLLC) which required a minimum space while maintaining high efficiency and flexibility.

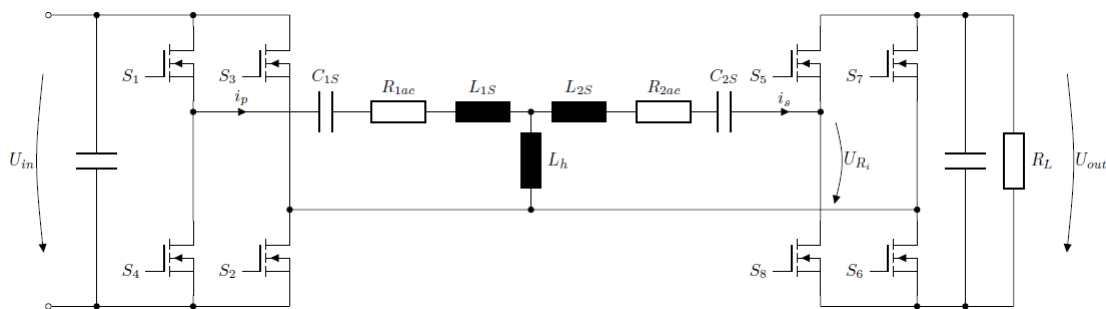


Figure 2.5: the CLLLC topology described in [16]

Gongjun *et al* in [11], in their paper researched about many types of structure for inductive coils and metal plates. In their paper, space spiral coils and parallel plates are formally approved without losing its generalization, and the mutual inductance and plate equivalent capacitance can be calculated. Gongjun and his colleagues proposed in this paper a dual-coupled robust WPT system (electric-coupled mechanism and magnetic-coupled mechanism) based on parity time (PT)-symmetric model, where the two main categories of coupling mechanisms in wireless power transfer are adopted to intensify the transfer efficiency and a parity time-symmetric circuit is used to bring about the system robustness of their results. The coupled-mode model is built to describe the system with the intention of studying the system's performance. If the dual coupled-mode is compared with single-coupled systems, it

is obvious that this scheme can give rise to a constant-characteristics power transfer with even a longer distance.

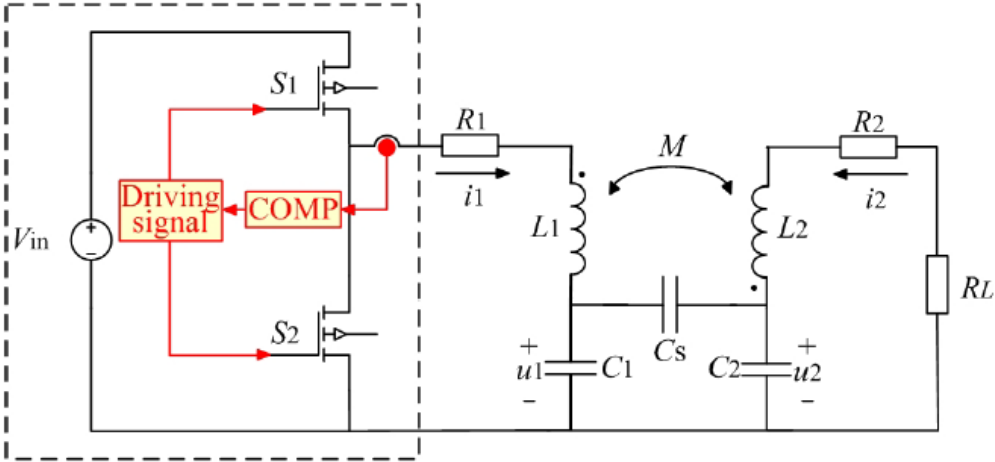


Figure 2.6: the equivalent circuit of the dual-coupled robust WPT system described in [11]

3 METHODOLOGY

The basic wireless charging technology topology for small electric vessels includes, a DC power source, an inverter, a resonant tank, inductive coils which are represented by an isolated transformer, a rectifier, and a load (resistor). And these components are shown in the block diagram in Figure 3.1 below.

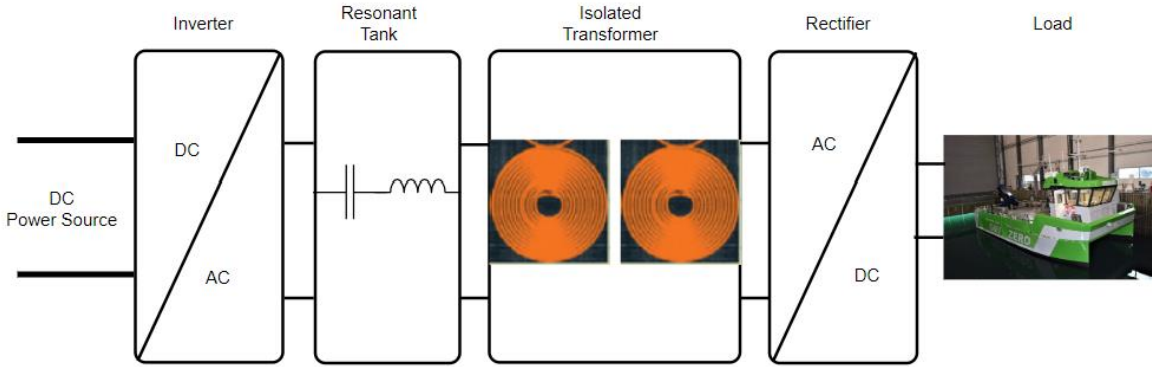


Figure 3.1: a block diagram of the Wireless Charger

In my project, a full bridge LLC resonant converter topology is used, and it is described in next subsections. Figure 3.2 shows my full bridge LLC resonant converter with a full-bridge rectifier at the secondary side. The input direct current (DC) voltage is inverted to an alternating current (AC) with the help of a full bridge inverter circuit, the switching bridge generates a square waveform to excite the resonant tank circuit which consists of L_r , C_r , L_m . The resonant tank is connected to an isolated ideal transformer which serves as the inductive coupler in the simulation, the secondary side of the isolated transformer is connected to a full-wave rectifier which rectifies the AC into a DC; the output capacitor filters the rectified AC current ripple and the voltage from the full-wave rectifier output is supplied to the load which is a resistor.

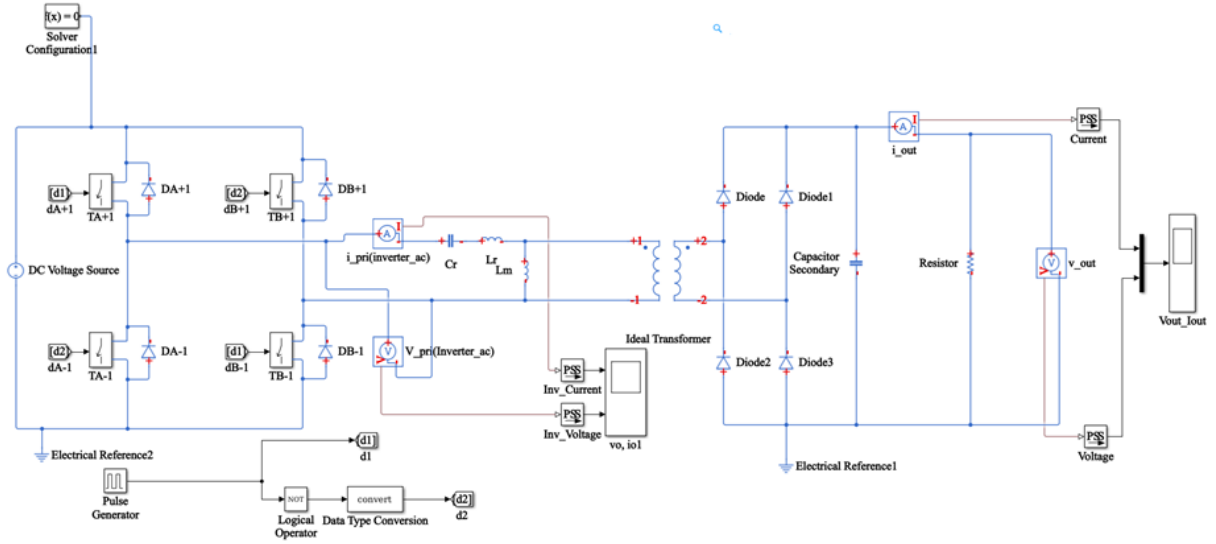


Figure 3.2: a full bridge LLC converter circuit with a boost converter in the secondary side

The characteristics of this isolated DC-DC converter depends majorly on two resonant frequencies which can be found in equation (3.1) and equation (3.2) as retrieved from the literature in [22]:

$$f_{r1} = \frac{1}{2\pi\sqrt{L_r C_r}} \quad (3.1)$$

$$f_{r2} = \frac{1}{2\pi\sqrt{(L_r + L_m)C_r}} \quad (3.2)$$

The DC converter characteristics moves close to the resonant frequency f_{r2} during light loading condition and during heavy loading condition, the peak characteristic of the DC converter goes close to f_{r1} .

Most people would rather have MOSFETs for the design of an LLC resonant converter, simply because it permits the operation of high frequency making sure that there is less switching loss and this can be achieved by choosing the optimum values for L_m , L_r and C_r . [22]. But in this project, I used IGBT's for the software simulation in MATLAB & Simulink, and MOSFETs for my hardware implementation. First, this is a matter of personal preference and because my converter hardware is already embedded with the MOSFETs. Secondly, my laboratory setup is for a small application, and IGBT's are mostly preferred for heavy or high applications.

Because a resonant LLC converter has many wanted features such as high efficiency, low Electromagnetic interference (EMI) and high-power density, the design of a resonant converter is challenging, and it requires more attempts to achieve an optimum operation as compared to a PWM converter [29]. As it will be explained in section 3.3 below and like I have done with some calculations in section 3.5 below in this project to simplify the challenges and make it easier to calculate the optimal values in designing the resonant tank.

Section 3 describes an overview of the wireless charger operation in its different mode of operation with a comprehensive design example along with its schematics.

3.1 Converter Voltage Gain

The voltage gain of the converter = switching bridge gain * resonant tank gain * transformer turn ratio (N_s/N_p). The gain of the switching bridge for a full-bridge inverter is 1 and that of the half bridge inverter is 0.5.

The gain of the resonant tank can be calculated by doing the analyses of the equivalent resonant circuit that is shown in Figure 3.3, the gain of the resonant tank is the magnitude of the transfer function as written in Eq (3.3) which was retrieved from [29].

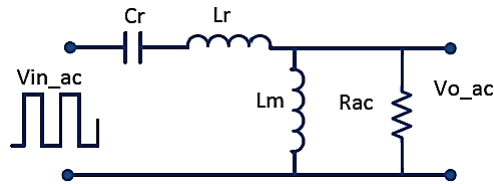


Figure 3.3: the equivalent resonant circuit

$$K(Q, m, F_x) = \left| \frac{V_{oac}(S)}{V_{inac}(S)} \right| = \frac{F_x^2(m-1)}{\sqrt{(m * F_x^2 - 1) + F_x^2(F_x^2 - 1)^2(m-1)^2Q^2}} \quad (3.3)$$

Where,

Impedance (Z_r):

$$Z_r = \sqrt{L_r/C_r} \quad (3.4)$$

Quality factor (Q):

$$Q = \frac{\sqrt{L_r/C_r}}{R_{ac}} \quad (3.5)$$

Reflected load
resistance (R_{ac_min}):

$$R_{ac_min} = \frac{8}{\pi^2} * \frac{N_p^2}{N_s^2} * R_o \quad (3.6)$$

Inductance ratio (K):

$$K = \frac{L_m}{L_r} \quad (3.7)$$

Magnetizing
Inductance (L_m):

$$L_m = \frac{R_E}{2\pi f_r} \quad (3.8)$$

$$L_p = \frac{(k + 1)^2}{(2k + 1)} L_r$$

Resonant inductor
(L_r):

$$L_r = \frac{1}{(2\pi f_o)^2 C_r} \quad (3.9)$$

Resonant Capacitor
(C_r):

$$C_r = \frac{1}{(2\pi f_r)^2 L_r} \quad (3.10)$$

$$C_r = \frac{1}{2\pi Q * f_o * R_{ac}}$$

Resonant Frequency
(f_r):

$$f_r = \frac{1}{2\pi \sqrt{L_r C_r}} \quad (3.11)$$

Normalized
switching Frequency
(F_x):

$$F_x = \frac{f_s}{f_r} \quad (3.12)$$

Ratio of Total Primary
Inductance to Resonant
Inductance (m):

$$m = \frac{L_r + L_m}{L_r} \quad (3.13)$$

You can plot the gain of the resonant tank K with the normalized switching frequency to get different values of Q (the quality factor) and any single value of the static parameter (m). Figure 3.4 shows that each gain curve has its own value which is used to give definition to the demarcation between the inductive and capacitive impedances of the resonant tank, hence the inductive and capacitive region is highlighted in the plot in Figure 3.4. It is important to define the inductive and capacitive region because our goal is to maintain a smooth operation

in the inductive region across the whole input voltage and the various range of current of the load without falling into the capacitive operation region. This type of requirement necessary because the Zero Voltage Switching (ZVS) can only be attained in the inductive region, also, operation in the capacitive region means that the current is leading the voltage, then the current in the MOSFET/IGBT will flow in the reverse direction before the MOSFET/IGBT turns off. After the MOSFET/IGBT turns off, the reverse current will flow in the diode of the MOSFET's body, this will cause a body diode hard commutation when the other half MOSFET in the inverter bridge is turned on, and as a result of this will also cause a reverse recovery losses and noise, and might cause high current spikes and device failure. [29]

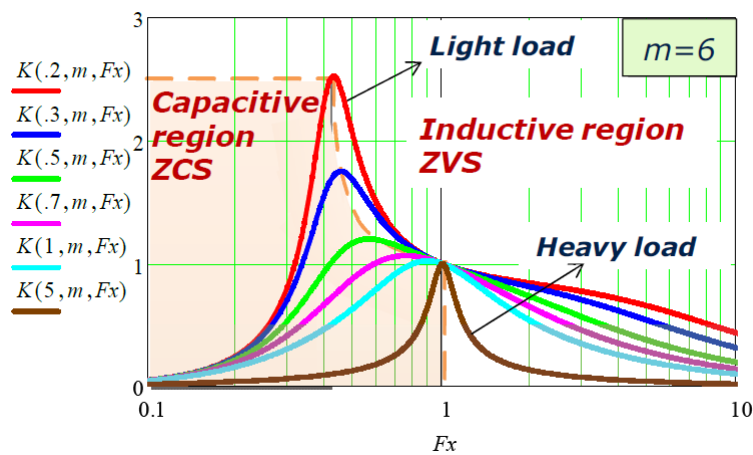


Figure 3.4: the gain curves [29]

3.2 Modes of Operation

Since the gain of the LLC network is frequency modulated, there are three modes in which the converter can be operated which depends on the input voltage and the condition of the current. The three modes are listed below and shown in Figure 3.5

- 1) When switching/operating frequency is equal the resonant frequency $f_s = f_r$.
- 2) When switching frequency is greater than the resonant frequency $f_s > f_r$.
- 3) When switching frequency is less than the resonant frequency $f_s < f_r$.

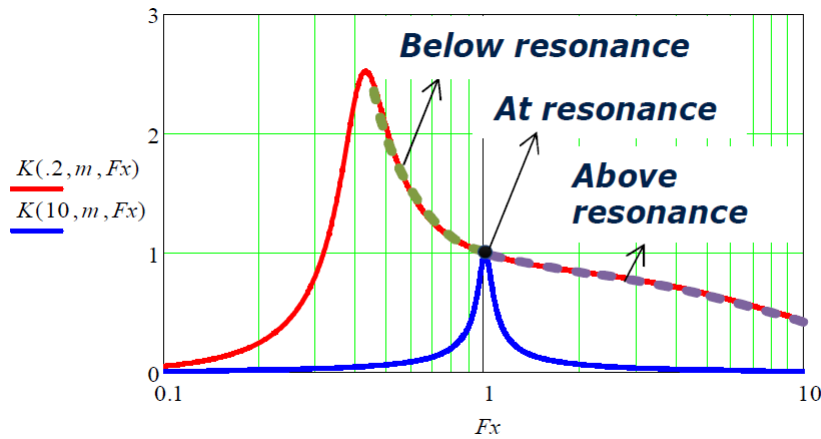


Figure 3.5: the converter's three modes of operation [29]

The converter has only two practicable operations in the cycle of switching which are described below. Note that the modes in 1, 2, and 3 mentioned above may be made up of one or both operations of the switching cycle.

- 1) The power delivery operation: this happens two times during the switching cycle when there is a positive voltage excitation in the resonant tank which causes the resonating current to flow or move in the positive direction in the first half of the switching cycle. And secondly, in the second half of the switching cycle when there is a negative voltage excitation in the resonant tank which causes the resonating current to flow in the negative direction. The equivalent circuit of the positive and negative voltage excitation are shown in Figure 3.6 and Figure 3.7 respectively. The magnetizing inductor voltage is the positive or negative reflected output voltage while the magnetizing current is the charging or discharging during the power delivery operations, and the difference in the resonant current from the magnetizing current flows through the transformer and full-bridge or half-bridge rectifier which in turn delivers power to the load.

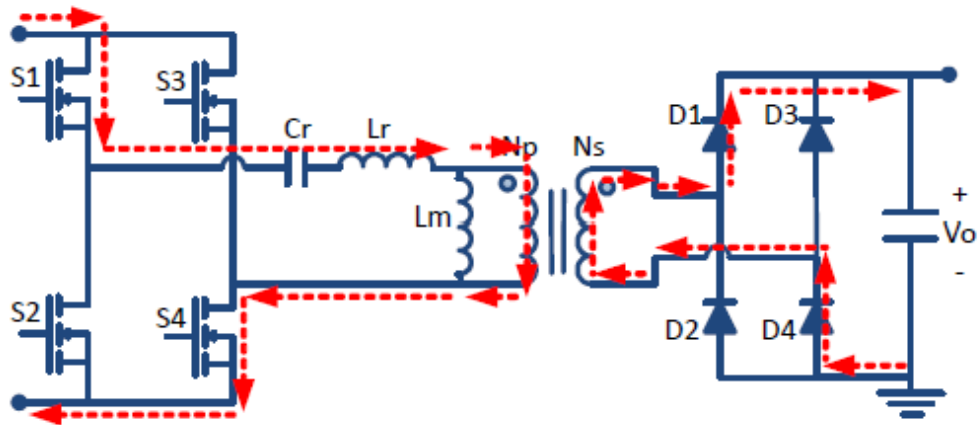


Figure 3.6: first half of switching cycle in positive direction [29]

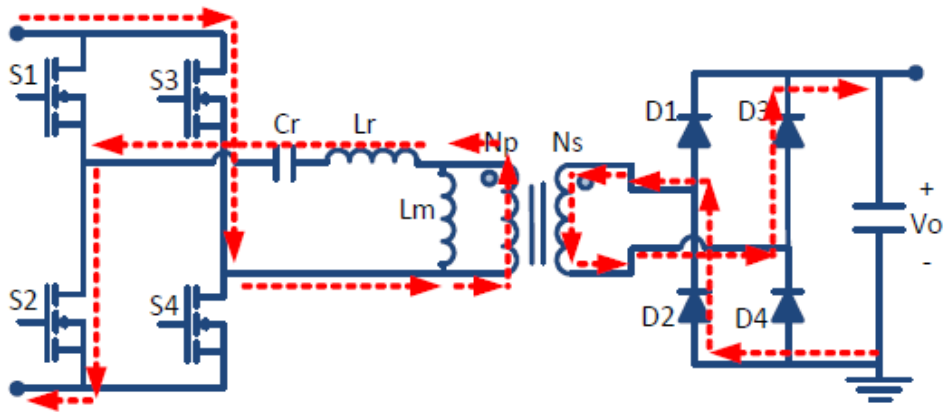


Figure 3.7: second half of switching cycle with negative voltage and direction [29]

- 2) The freewheeling operation: this happens after the power delivery operation only in conditions when the resonant current gets to the same level as the transformer magnetizing current, i.e. when $f_s < f_r$ which causes the transformer secondary current to get to zero and in turn disconnect the secondary side rectifier circuit. The consequence of this occurrence is the free entrance of the magnetizing inductor to resonance with the resonant inductor and resonant capacitor. The frequency of the second half resonance is smaller than the initial resonant frequency, mostly at high values of m where L_m is far greater than L_r ($L_m \gg L_r$), thus the primary current during the freewheeling operation will only change slightly and can be approximated to be unchanged for simplicity. Figure 3.8 and Figure 3.9 shows each half switching cycle of the freewheeling operation.

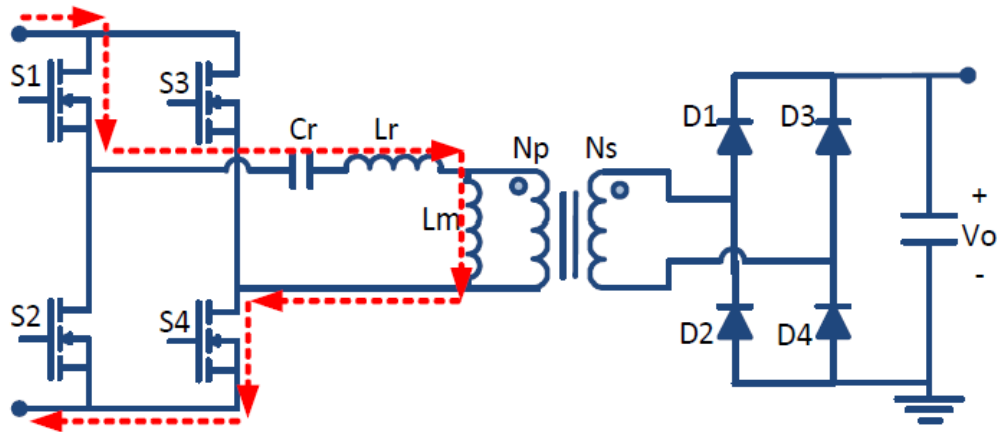


Figure 3.8: first half of freewheeling [29]

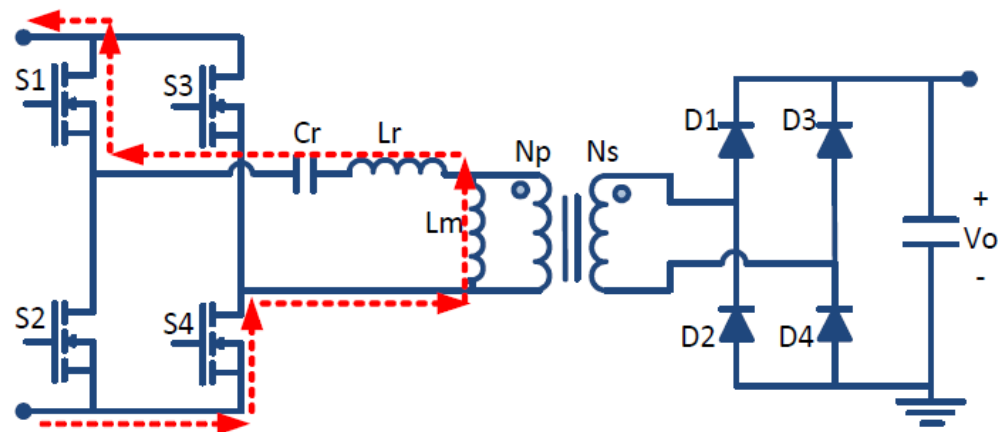


Figure 3.9: second half of freewheeling [29]

3.2.1 Switching/operating frequency is equal the resonant frequency $f_s = f_r$

When the resonant half cycle during each switching half cycle is complete in the power delivery operation describe in 1) above, the resonant inductor current I_{Lr} reaches the magnetizing current I_{Lm} , and the current that flows through to the secondary side rectifier reaches zero. Then the optimized operation and efficiency of the resonant tank is at its best because it will be at a unity gain; the transformer turns ratio is selected to suite the converter operation at nominal input and output voltages.

3.2.2 Switching frequency is greater than the resonant frequency $f_s > f_r$

When each switching half cycle is complete, it consists of a partial power delivery operation which is almost identical to the operation of the resonant frequency. But it differs in the sense

that the resonant half cycle is not completed and it is interrupted as at the time the other half cycle will be starting, hence the MOSFETs in the inverter side of the converter will get an increase in turn off losses and the diodes in the rectifier side will have hard commutation. This mode is commonly operated in the converter when there is higher input voltage and a step-down gain, or a buck is needed.

3.2.3 Switching frequency is less than the resonant frequency $f_s < f_r$

When each switching half cycle is complete, it consists of a power delivery operation which was described in 1) above and when the resonant half cycle is also complete, the resonant inductor current I_L reaches the magnetizing current, and the operation of the freewheeling which was described in 2) above begins and it keeps on with the operation till the end of the switching half cycle, hence, due to this circulation of energy, there will be an increase in conduction losses on the primary side. This mode is commonly operated in the converter when there is lower input voltage and a step-up gain, or a boost is needed.

3.3 Design Steps

This segment describes the influence of the parameters of design on voltage regulation and efficiency performance, and it makes the design and selection of such parameters easier to know and implement. My priority here is to successfully bring about the best performance at the same time achieving the requirements of the gain for all load and line conditions. And I must find out the least switching frequency the controller shall limit to be certain the entire operation will be in the induction region and not the conductive region.

Below are five steps which will explain the decisions to take when making your design parameters and selection, and Figure 3.10 shows a design flow chart which is summarized for the design methodology.

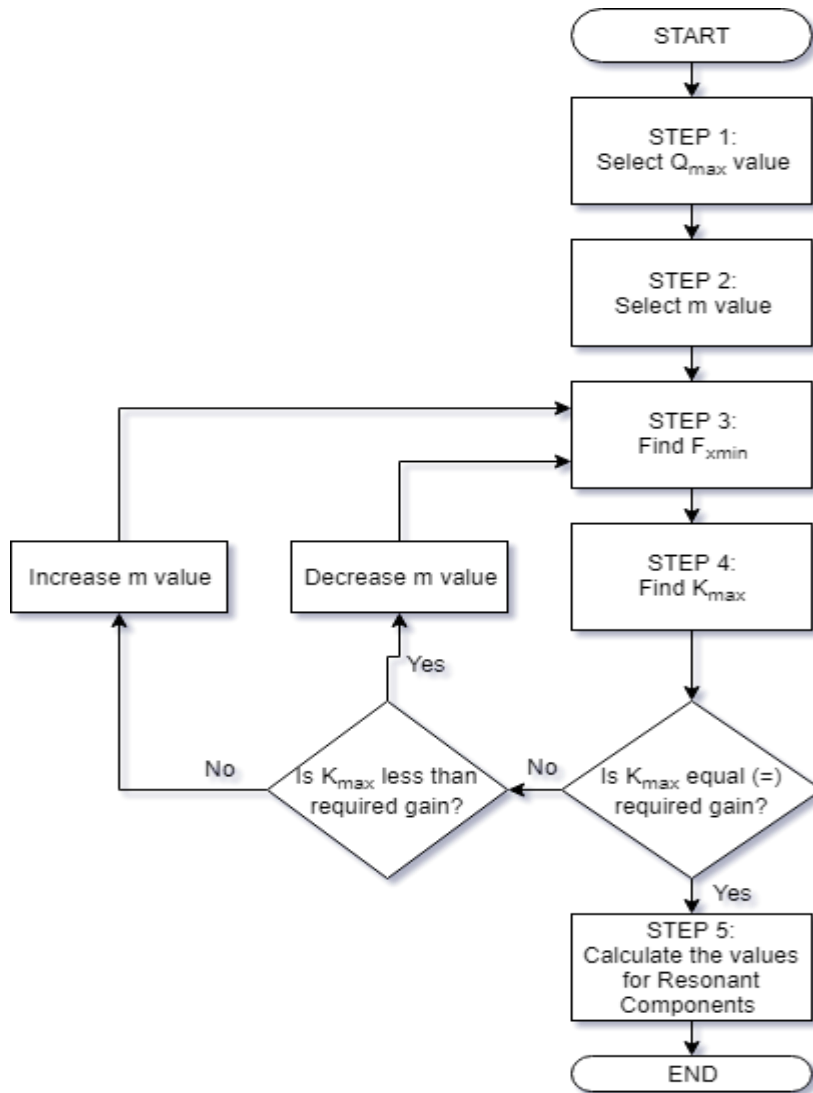


Figure 3.10: design flow chart

3.3.1 STEP 1: Selecting the Q_{max} Value

From Equation (3.5), we can see the quality factor which is dependent on the current of the load. When heavy loads are operated, the values of Q are high, while the values of Q are lower during the operation of lighter loads. It is important to set a maximum value for Q (i.e. Q_{max}) to match with the maximum load condition.

To understand the phenomenon Q value has on voltage gain/regulation, a graphical illustration is shown in Figure 3.11, which plots the voltage gain (k) for different values of Q . Based on assumption, if the resonant tank gain ranges from 0.8 to 1.2 for example, it can be seen that the low Q curve ($Q=0.3$) with legend colour of red can achieve a higher boost gain, but it is less sensitive to frequency modulation as described in 3.2.2 above ($f_s > f_r$ region),

therefore, the switching frequency will have to increase much in order to achieve the minimum voltage gain ($K=0.8$), which leads to additional switching losses, while the higher Q value curve ($Q=1$) can achieve the minimum gain ($K=0.8$) with lesser increase in the switching frequency, but the higher Q value is unable to get to the maximum gain ($K=1.2$). Hence, a normal Q value of about 0.5 seems to satisfy the voltage gain requirement in this situation/problem. [29]

In conclusion, by adjusting the Q value one can achieve the maximum gain but the side effect is that frequency modulation range will be increased. Therefore, one cannot depend on tweaking the value of Q_{max} when doing the design iteration so that one may reach the maximum voltage gain desired, but one should depend on tweaking the m value which will be described in 3.3.2 below.

Even though there is not a straightforward way of selecting the best and appropriate value of Q , one must choose moderately the value of Q_{max} which is mentioned above and based on a specific design available.

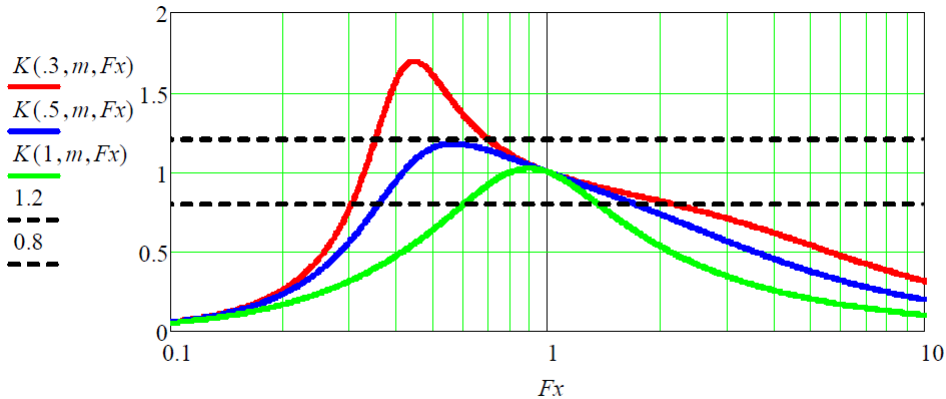


Figure 3.11: the voltage gain plot with different values of Q [29]

3.3.2 STEP 2: Selecting m value

As written above in equation (3.13), $m = \frac{L_r + L_m}{L_r}$ is a static parameter which we must begin its design by making the most effective use of its value, hence, it is of great significance to comprehend the influence of the ratio m on the converter operation. To put on a graphical display of the influence the value of m has on the converter operation, Figure 3.12 shows the same resonant tank voltage gain plots as illustrated in page 25 (Figure 3.11) but for individual values of m such as: $m = 3$, $m = 6$, and $m = 12$. It is evident that smaller m values can attain

higher boost gain, in addition to the smaller range of the frequency modulation, meaning more flexible control and regulation, which is precious in applications which have wide input voltage range. Despite this, low m values attached to the same quality factor Q and resonant frequency f_r indicates a smaller magnetizing inductance L_m , hence, a greater or elevated magnetizing peak-peak current ripple, which causes an increase in the circulating energy and losses during conduction.

You must choose a logical initial m value (maybe from 5 - 10), and then make the best and most effective use it by working on a few iterations to obtain the maximum value of m that can still attain the maximum gain desired for different conditions of load.

Table 3.1: the comparison between high and low m value

Low m value	High m value
Higher boost gain	Higher magnetizing inductance
Narrower frequency range	Lower magnetizing circulating current
More flexible regulation	Higher efficiency

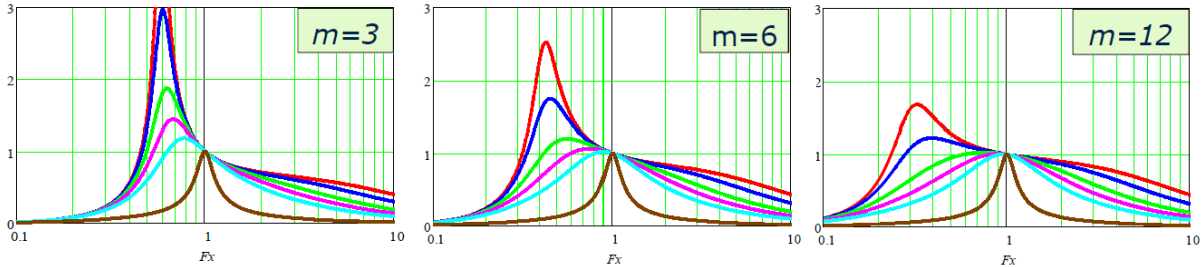


Figure 3.12: the same resonant tank gain plots but different m values [29]

3.3.3 STEP 3: Finding the Least Normalized Switching Frequency

When the value of Q_{max} has been selected and an initial value form is defined, it is essential to find the value of the least normalized switching frequency which can guarantee the maximum load condition (Q_{max}) in the inductive operation. Not just for Q_{max} but for all other loads as well.

The least normalized switching frequency can be obtained at the peak gain in the Q_{max} curve. This can be calculated using equation (3.14) (let's assume $Q_{max}=0.4$ and $m=6.3$ as an example)

$$\left. \frac{d}{dF_x} K(Q, m, F_{x_min}) \right|_{Q_{max}=0.4, m=6.3} = 0 \quad (3.14)$$

Solve for F_{x_min}

3.3.4 STEP 4: Voltage Gain Verification (K)

To confirm that the maximum gain (K_{max}) reached during maximum load by the chosen m value is enough, we must solve using the equation in (3.15) below.

$$K_{max} = K(Q_{max}, m, F_{x_min}) \quad (3.15)$$

After some iterations are done, one can achieve the design optimization which is shown in the design flow chart in Figure 3.10 above. If K_{max} is not enough, then we must decrease the value of m and continue from steps 3 and 4 again, to obtain a higher boost gain. Whereas when K_{max} is greater than what is needed, then the value of m can be increased and then continue the calculation from steps 3 and 4 to achieve an optimized efficiency.

3.3.5 STEP 5: Calculating Resonant Components Values

When a few iterations of the design flow are done, and getting to the optimum value of m , one can advance to the calculation of the values of resonant tank components, equation (3.5) and equation (3.6) can be used to solve for L_r and C_r , and then L_m can be calculated using equation (3.13)

$$Q = \frac{\sqrt{L_r/C_r}}{R_{ac_min}} \quad (3.3)$$

$$R_{ac_min} = \frac{8}{\pi^2} * \frac{N_p^2}{N_s^2} * \frac{V_o^2}{P_{0max}} \quad (3.4)$$

$$f_r = \frac{1}{2\pi\sqrt{L_r C_r}} \quad (3.9)$$

$$m = \frac{L_r + L_m}{L_r} \quad (3.11)$$

Note that the selection of the resonant frequency f_r was not acknowledged in the design steps in 3.3 above, simply because it does not have any effect on the maximum gain and the operating region of the resonant converter. However, it is selected because the power density of the converter and the power losses of the converter are being considered.

3.4 Full-Bridge Inverter, Resonant tank and Full-bridge Rectifier Selection

A very sensitive decision in order to achieve the best converter performance is to rightly and carefully choose the bridge inverter (half-bridge or full-bridge) and rectifier (half-wave or full-wave) circuits.

3.4.1 Full-Bridge Inverter

The LLC converters usually are executed with a full-bridge or a half-bridge circuit on the primary side. The half-bridge inverter usually generates two times the current of what a full-bridge inverter would produce, with half the amount of switching as compared to a full-bridge. Even though a half-bridge consists of half of the primary number of turns for the same voltage gain and magnetic flux swing, and half of the primary winding resistance; the copper losses and conduction losses in the primary side are still two times that of a full-bridge simply because the squared rms current of the half-bridge is quadrupled. It is recommended to use a full-bridge switching circuit in applications that contains high primary currents, where conduction losses are having power and control over transfer of energy. [29]

So, in this project, I am used a full-bridge inverter in Simulink for my software and for my hardware, I used the full-bridge inverter embedded in the 'Drives board' from University of Minnesota and controlled by dSPACE control system; this will be discussed further below.

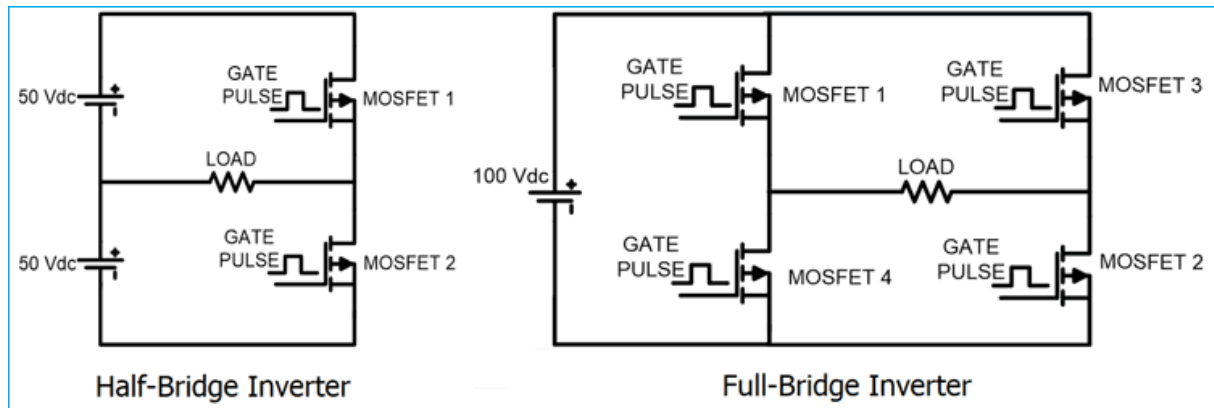


Figure 3.13: the half bridge and full bridge inverter circuit

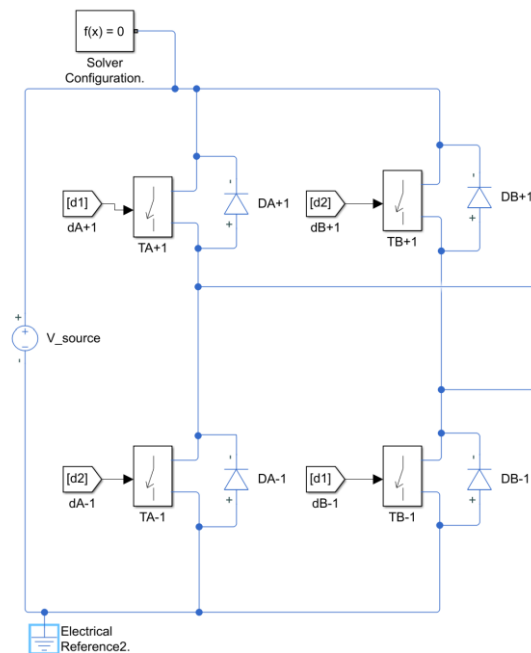


Figure 3.14: my Inverter Circuit with its resonant tank which I designed using MATLAB&SIMULINK

3.4.1.1 Circuit driving and analogue control of switching circuit

During the proper operation of the circuit, the the source voltage of the upper transistor changes with the output voltage. So, to succeed in driving the switches of these upper MOSFETs, certain driver chips are introduced in the circuit. A common analogue chip that is widely used is the IR2110 which has a 10V or 12V voltage between the gate and source. Therefore, the switches are allowed to operate simultaneously using the feedback signal from the IR2110's output. In addition to this, a MC34066 (high performance resonant mode controller) analogue chip is also included in the switching circuit to regulate the converter's output voltage and to modulate the switching frequency through fixed on-time or off-time control. This particular high-performance controller's core components include an output

circuit, a variable frequency oscillator, an error amplifier, a reference voltage, and a soft-start circuit. [19]

In [22], unlike in [19] described above, the IR2110 chip is used in combination with the ATMEGA8 microcontroller which generates pulses and modulate switching frequency for the MOSFETs. The AVR was used to programme the ATMEGA8 microcontroller.

In this project, I used the IR2133 chip in driving my MOSFETs which is embedded in the ‘Drives board’, a converter board from University of Minnesota; and I controlled the converter using dSPACE module. The IR2133 is a high voltage, high speed power MOSFET and IGBT driver with three independent high side and low side referenced output channels for 3-phase applications. I only used a single phase-two leg out of the three phases to make a full-bridge inverter which was all I needed, and I generated the PWM signals to control the MOSFETs from an external source. The switching delays are matched to simplify use in high frequency applications. The floating channels of the IR2133 can be used to drive N-channel power MOSFETs or IGBTs in the high side configuration which operates up to 600 volts or 1200 volts. It has a VCC Fixed supply voltage 10V or 12V, and 20V at maximum. [30]

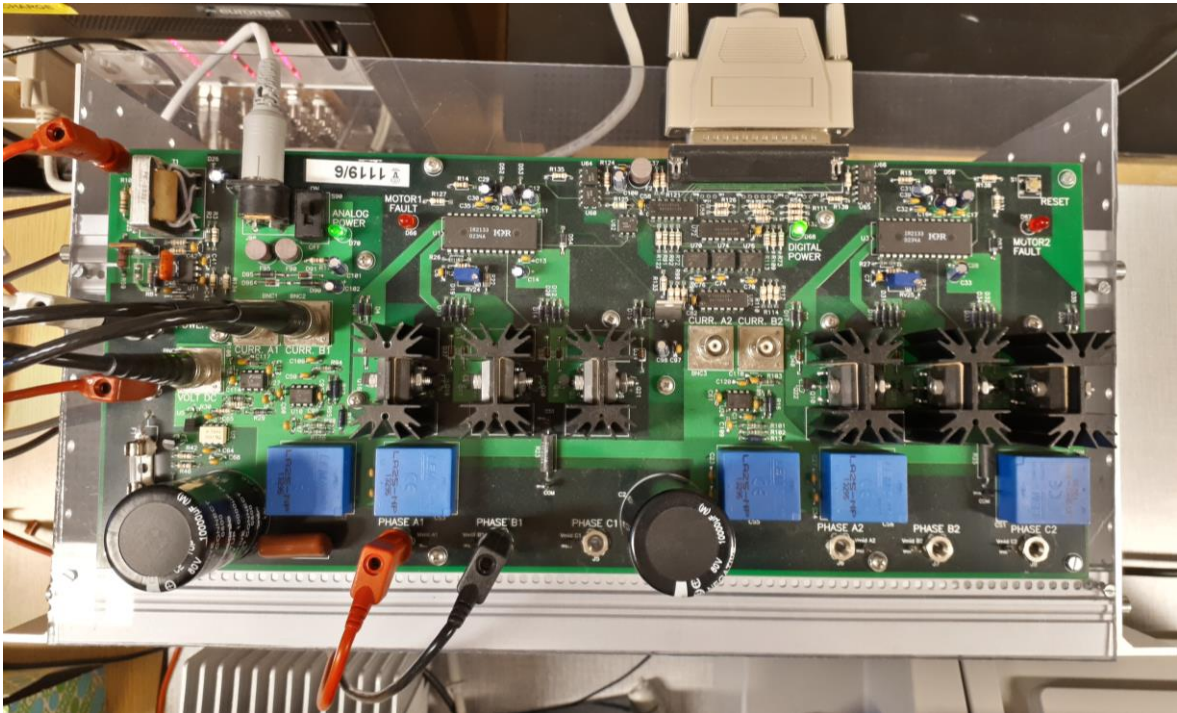


Figure 3.15: the Drives board from University of Minnesota for the Inverter Circuit (primary side)

3.4.2 Resonant Tank

MOSFETs achieves a ZVS condition in their turn-on transition when the operating frequency is higher than the frequency at the peak voltage gain of the LLC resonant tank with different load conditions. To make an adequate preparation for ZVS condition, the presence of an inductive impedance is important because the resonant current needs to lag the supply voltage. The magnetizing inductor L_m is expected to be able to provide the essential amount of inductive energy needed. The L_m value is chosen such that the value of the magnetizing current is not meant to be 20% higher/larger than that of the resonant current. The value of L_m is meant to be high so as to have a decrease in the conduction losses and the same time, the value of L_m should be selected as low as possible so as to achieve a successful ZVS. This LLC resonant tank is composed of series resonant capacitor C_r , series resonant inductor L_r , parallel resonant inductor L_m and an equivalent load resistor R_{eq} . [22]

3.4.3 Full-Bridge Rectifier

A Full bridge rectifier is a type of full wave rectifier that makes use of both half cycles of input alternating current (AC) and converts them to direct current (DC). A bridge rectifier is convenient and acceptable for applications that involve high voltage because of its high peak inverse voltage (PIV). At any point when the voltage at the transformer secondary reaches positive peak value V_{max} , diodes D1 and D2 will be forward biased (conducting) and the diodes D3 and D4 will be reverse biased (non-conducting). And if we take into account ideal diodes in full-bridge, D1 and D2 which are forward biased will have a resistance of zero. Which means that the reduction in voltage across the conducting diodes (D1 and D2) will be zero. This means that all the voltage that is produced in the transformer secondary goes to the resistance of the load (R_L).

Thus, the PIV of a full-bridge rectifier = V_{max} (max of secondary voltage) [32]

Connecting a capacitor or an inductor across the load can smooth the output voltage of a full-Wave rectifier. [18]

The LLC converters can also be put into practice with the addition of a full-bridge or a full-wave rectifier circuit on the secondary side, as shown in Figure 3.16. During the first half cycle of the input voltage, the diodes D1 and D2 are forward biased and current flows through D1 and enters the load resistance R_L and returns back flowing through D2. During this whole

process, D3 and D4 are reverse biased and current is not allowed to flow through them. The flow of current is indicated by solid arrows in the Figure 3.16 below.

During the second half cycle of the input voltage, the diodes D3 and D4 become forward biased and current flows through D3 and enters the load resistance R_L and returns back to the transformer secondary flowing through D4. During this whole process, D1 and D2 are reverse biased and current is not allowed to flow through them.

Note: the green arrows indicate the beginning of current flow from the transformer secondary to the load resistance and the red arrows indicate the return path of current from load resistance to the transformer secondary, thereby making the circuit complete.

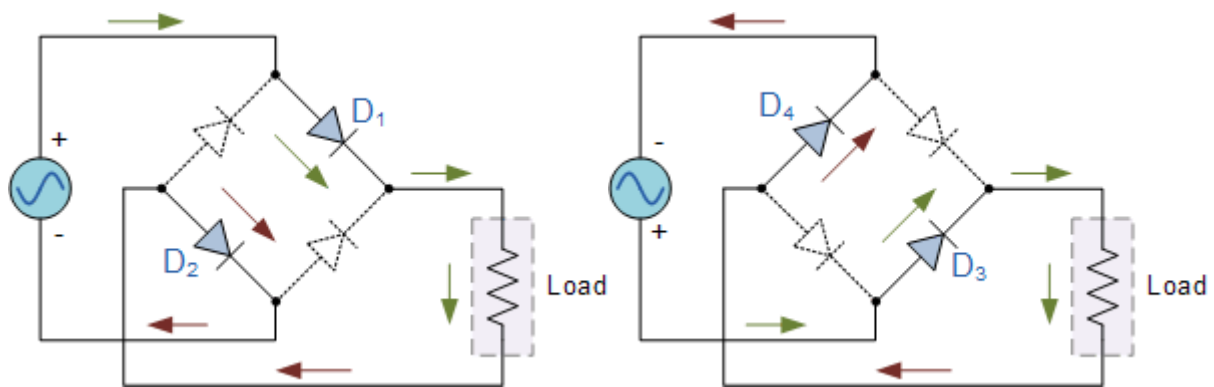


Figure 3.16: the positive and negative half cycle of a full-bridge rectifier

3.4.3.1 Advantages of a Full-wave rectifier over a half-wave rectifier

- Efficiency is double for a full wave bridge rectifier. The reason is that, a half wave rectifier makes use of only one half of the input signal. A bridge rectifier makes use of both halves and hence double efficiency
- The residual ac ripples (before filtering) is very low in the output of a full-bridge rectifier. The same ripple percentage is very high in half-wave rectifier. A simple filter is enough to get a constant dc voltage from the full-bridge rectifier.
- The efficiency of full-bridge is double that of the half-wave rectifier which means higher output voltage and power, Higher transformer utilization factor (TUF). [32]

Figure 3.17 below shows my constructed full-bridge rectifier which has a capacitor connected in parallel for filtering to get a smooth output voltage and a linear voltage regulator (L7812CV) connected in parallel to the capacitor to get a near 12 v DC output.

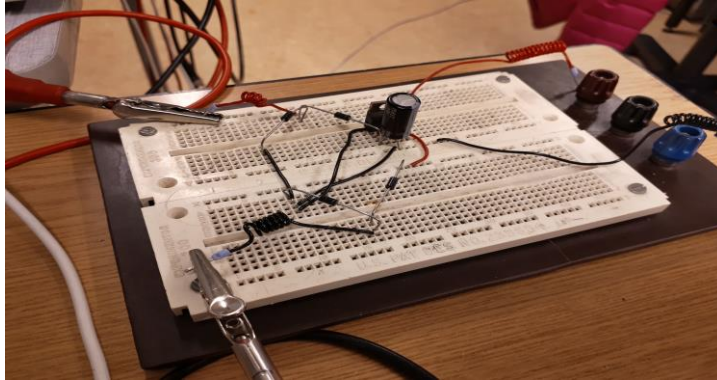


Figure 3.17: my full-bridge rectifier

3.5 Design Example and Calculation

3.5.1 Application and Specifications

Table 3.2: the target specification for the heavy load and light load

Item	For Heavy Load	For Small Application
Input voltage, V_{in}	400V DC	12V DC
Output voltage and current V_o, I_o	600V DC, 1.7A	11.1V DC, 1.5A
Output power, P	1020W	16.7W
Efficiency, η	>98%	>98%
Resonant frequency, f_r	115kHz	50kHz
Frequency range	56.5kHz - 150kHz	24.5kHz - 74kHz

3.5.2 Design Steps

3.5.2.1 Software

I started by calculating the transformer turn ratio n . And then calculate minimum and maximum voltage gains of the resonant tank in the case where you have varying input voltage. But in my application, I only have one input voltage; so, my nominal voltage gain will be the same as my minimum or maximum voltage gain.

$M_{nom}=1$ (simply because the switching bridge gain for a full-bridge is 1 and that of half-bridge is 0.5)

$$\frac{N_p}{N_s} = \frac{V_{in_{nom}}}{V_{out}} \cdot M_{nom} = 0.667$$

$$M_{max} = \frac{V_{in_{nom}}}{V_{in_{max}}} \cdot M_{nom} = 1$$

Following the steps in section 3.3 above:

Step 1: Let us choose the value of Q_{max} to be 0.4

Step 2: Let us choose the value of m to be 6.3

Step 3: you can calculate the minimum normalised switching frequency by solving the gain equation in Eq (3.3) above, simply by differentiating the values $K(Q_{max}, m, F_{x_{min}})$ from F_x i.e. $\frac{dK(Q_{max}, m, F_{x_{min}})}{dF_x}$, and it can also be found at the peak of the Q_{max} curve as given in the gain plot shown in Figure 3.18. Therefore,

$$F_{x_{min}} = 0.489$$

$$f_{s_{min}} = F_{x_{min}} * f_r = 56.24kHz$$

Step 4: this step is used to verify the voltage gain.

$$Q_{max@Vmin} = Q_{max} * \frac{V_{in_{min}}}{V_{in_{max}}} = 0.4.$$

But in the case of other applications where the power rating varies due to varying input voltage range, the value of Q_{max} will change with respect to the minimum and maximum voltage.

Therefore, we can calculate the maximum gain at the minimum switching frequency using equation (3.3) or we can find the equivalent value from the gain plot shown in Figure 3.18.

$$K_{max} = K(Q_{max@Vmin}, m, F_{x_{min}}) = 1.352$$

$$K_{max} = 1.352 > M_{max} = 1$$

So, there is no need to tune the value of m .

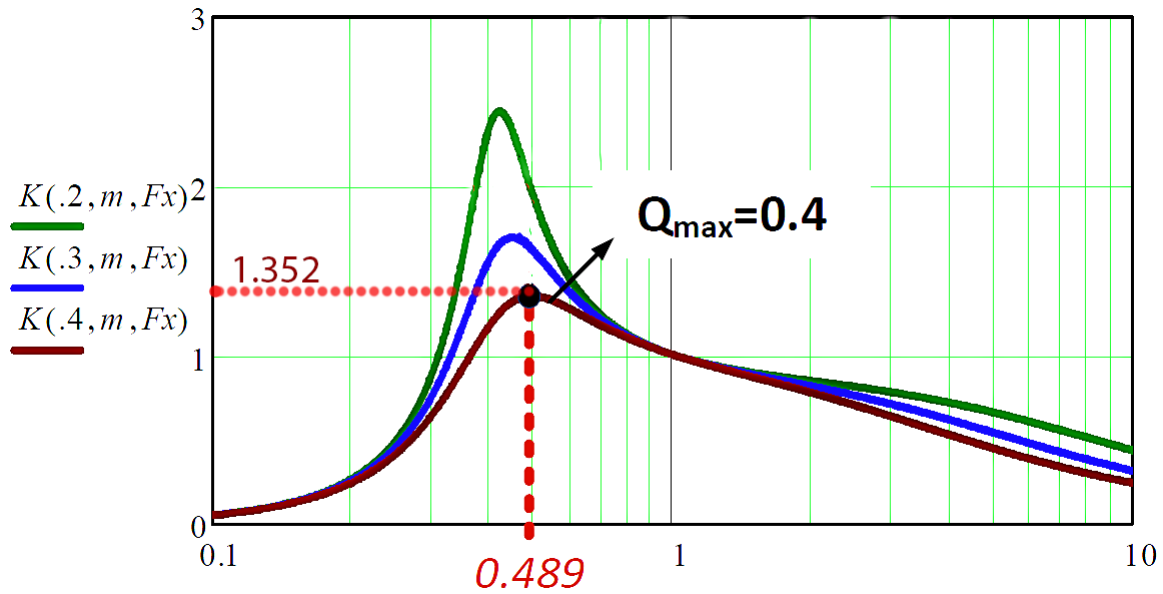


Figure 3.18: the gain plot [29]

Step 5: Now we calculate the values of the resonant components (L_r , C_r , and L_m).

At full load condition, the load resistance can be calculated as:

$$R_{ac_min} = \frac{8}{\pi^2} * \left(\frac{N_p}{N_s}\right)^2 * \frac{V_{out}^2}{P_{o,max}} = 128.4 \Omega$$

$$Q_{max} = 0.4 = \frac{\sqrt{L_r/C_r}}{128.4 \Omega}$$

$$f_r = 115 \text{ kHz} = \frac{1}{2\pi\sqrt{L_r*C_r}}$$

$$m = 6.3 = \frac{L_r+L_m}{L_r}$$

Therefore, after doing some basic mathematical calculations and substitution method. $C_r = 0.027\mu\text{F}$, $L_r = 71.2\mu\text{H}$, and $L_m = 377.2\mu\text{H}$

3.5.2.2 Hardware (for small application)

Here, I will skip some design steps as most of the information can be found in section 3.5.2.1 above and the parameters for this section can be found in Table 3.2.

Calculating the transformer turn ratio, $\frac{N_p}{N_s} = \frac{V_{innom}}{V_{out}} \cdot M_{nom} = 1.08$

Steps 1, 2, and 4 remains the same as done in section 3.5.2.1 above

Step 3: $f_{s_min} = 24.45 \text{ kHz}$

Step 5: $R_{ac_min} = 6.975 \Omega$

$$Q_{max} = 0.4 = \frac{\sqrt{L_r/C_r}}{6.975 \Omega}$$

$$f_r = 50 \text{ kHz} = \frac{1}{2\pi\sqrt{L_r*C_r}}$$

$$m = 6.3 = \frac{L_r+L_m}{L_r}$$

Therefore, after doing some basic mathematical calculations and substitution method. $C_r = 1.14 \mu\text{F}$, $L_r = 8.88 \mu\text{H}$, and $L_m = 47.05 \mu\text{H}$

3.6 Laboratory Setup Description

The drives board in Figure 3.15 which I used for my laboratory setup is designed to be able to perform a variety of experiments on AC/DC machines. The main features include: two completely independent 3-phase PWM inverters for complete simultaneous control of two machines, 42 V dc-bus voltage to reduce electrical hazards, digital PWM input channels for real-time digital control, and complete digital/analogue interface with dSPACE board.

I supplied a 15 v DC obtained from a DC power source to the drives board, to power the inverter driver circuit (IR2133) and also supplied a 42 v DC to power the whole board itself.

My BNC cable connections are as follows:

1. I connected the DSI: 37-pin dSub from the drives board to the Slave I/O PWM on dSPACE for control signals.
2. I connected the pin named CURR. A1 on the drives board to ADCH5 on dSPACE control system for phase A current.
3. I connected the pin named CURR. B1 on the drives board to ADCH6 on dSPACE control system for phase B current.
4. I connected the pin VOLT DC from the drives board to ADCH1 on dSPACE control

4 Coil Design

The system utilizes a high frequency power source to energize the transmitting coil which is fine tuned by an external capacitor to attain the required resonant frequency. A receiving resonant coil which is physically separated from the transmitting resonant coil thus captures the generated magnetic field through induction. A rectifier circuit then smoothens the received AC power before supplying it to the load.

The wireless power transfer (WPT) operates on the principle of magnetic resonant inductive coupling. The wide physical distance separation of the charging coils enables the strong coupling of the magnetic near fields of these coils when finely tuned. This implies that, the efficient transfer of energy from the transmitter to the receiver coils is achieved at resonance by magnetic coupling.

4.1 Theoretical Analysis

The efficiency of the transferred power is dependent on the absorbed power by the transmitter coils (P_1), the received power by the receiver coil (P_2) and the delivered power by the receiver coil to the electric load resistance (P_L). The efficiency of the WPT system can therefore be expressed as the ratio of the output power (delivered power by the receiver coil to the load resistor) to the source power of the system (the total delivered power from the source to the system). This can be expressed mathematically as shown in equation (4.1), as retrieved from [23]:

$$\eta_{12} = \frac{P_L}{P_1 + P_2 + P_L} \quad (4.1)$$

The efficiency of the transferred power also depends on other physical factors such as the frequency, number of turns of the coil structure, the coil radius, distance between the coils, and the material property of the coils. The efficiency of the transferred power reduces if the system operates at frequencies other than the required resonance frequency due to a reduction in the mutual inductance as a result of increasing vertical coil separation. Each vertical gap between the coils contains one resonant frequency. Due to the strong magnetic field coupling, two resonance points can be observed for smaller distances. It is therefore important to understand that, the strong coupling points where maximum efficiency can be achieved varies from one system to another. It is therefore required to determine an optimal coil gap

considering the operating frequency in order to design and build an efficient power transfer system for wireless electric vessels. [23]

4.2 LITZ wire

Litz wires are made up of several rope-like single insulated wires bunched together and are utilized in electrical systems that require good flexibility and high frequencies.

High frequency litz wires are made by using several single strands of wires that do not make electrical contact with each other and are usually utilized in applications with operation frequencies between 10kHz and 5MHz. Increasing frequencies cause current to flow over the surface area of the conductor, this phenomenon is known as “skin effect”. Similarly, reducing the cross-sectional area of the conductor also results in a decrease in the current flow across the cross-section of the conductor even at high frequencies. These losses at high frequencies are due to “proximity effect”, where there is a negative effect of the neighbouring electrical fields on the electromagnetic distribution. The twisted construction of litz wires consisting of multiple insulated conductor aids in the effective minimization of these high frequency losses.

The insulated single wires are the basic components of a litz wire. To achieve optimal results, a conductor material and an enamel coating can be combined to satisfy the requirements of specific applications. Figure 4.1 shows the diameter of a standard litz wire.

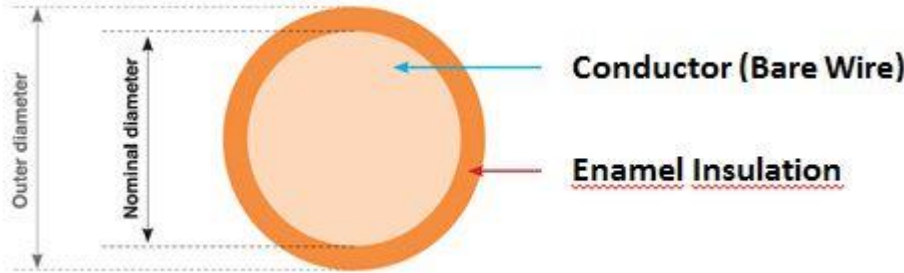


Figure 4.1: the diameter of a standard Litz wire [25]

In this project, I used an unserved basic high frequency Litz Wire because of its preferred properties such as the cost-effective design, resistance or frequency-related construction, increased tensile strength, high conductivity, and high bending cycle behaviour. This wire has an insulating coating which prevents from short-circuit when winding the wires around one another [25]. It can be used in several applications such as inverters, RF transformers, medical application, RF chokes, inductive charging and the likes to decrease the power losses that

transpires as a result of eddy current and also to decrease the skin effect. The operating frequency of each application determines the parameters of the litz wire, and it also determines the diameter of a single wire that should be used. The higher the operating frequency of the inductive components, the smaller the diameter of a single wire selected. [26]

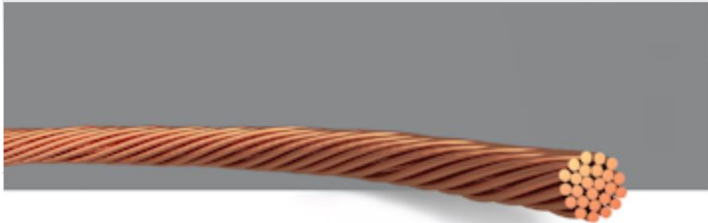


Figure 4.2: a typical unserved basic Litz Wire [25]

4.2.1 Choosing number and diameter of strands

A four-step approach was used in choosing the number of strands and diameter of the litz wire and this approach can be summarized as shown in Figure 4.3.

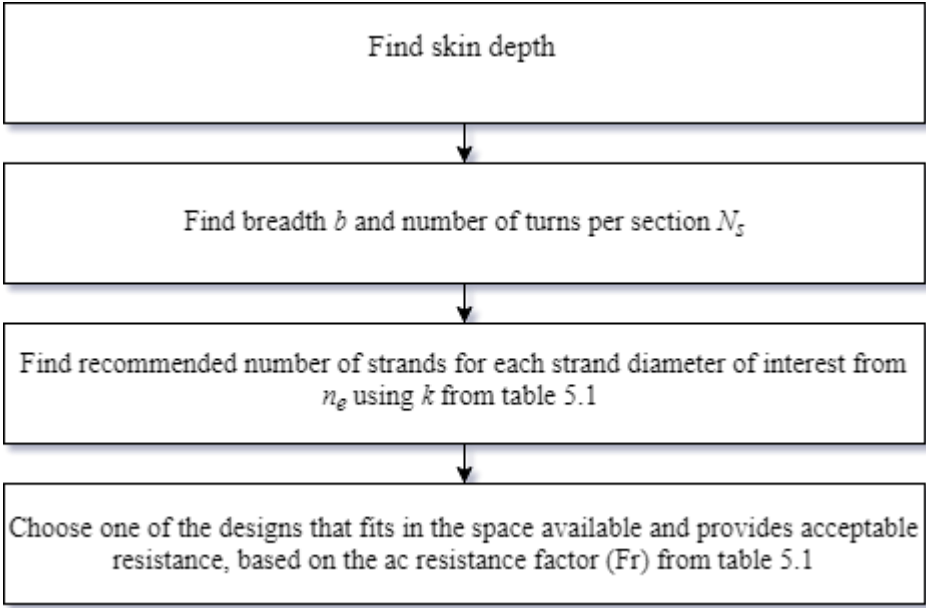


Figure 4.3: the flowchart of the Litz Wire design steps

1. Find skin depth: The skin depth can be expressed as

$$\delta = \sqrt{\frac{\rho}{\pi f \mu_0}} \tag{4.2}$$

Where:

ρ = the resistivity of the conductor ($1.72 \times 10^{-8} \Omega \cdot m$ for copper at room temperature, or $2 \times 10^{-8} \Omega \cdot m$ at $60^\circ C$)

f = The sinusoidal frequency current, and

μ_0 = permeability of free space ($4 \times 10^{-7} \pi$ H/m).

Applying MKS system of units to the variables in the equation leads to a calculated skin depth in meters.

2. Winding parameters:

The winding parameters that needs to be calculated are b and N_s , as illustrated in Figure 4.4 for some common winding geometries. b denotes the breath of the winding along the surface where the windings faces each other, and N_s represents the number of turns of the windings. In basic windings where there is no interleaving, N_s is the number of turns of the designed winding ($N_s = N$). Where interleaving is involved, it is the number of turns starting from a zero-field surface to the face underlining the primary and secondary. The zero-field surface lies either against a high-permeability core, or when the design in symmetrically interleaved, the zero-field surface will be located at the centre of the windings.

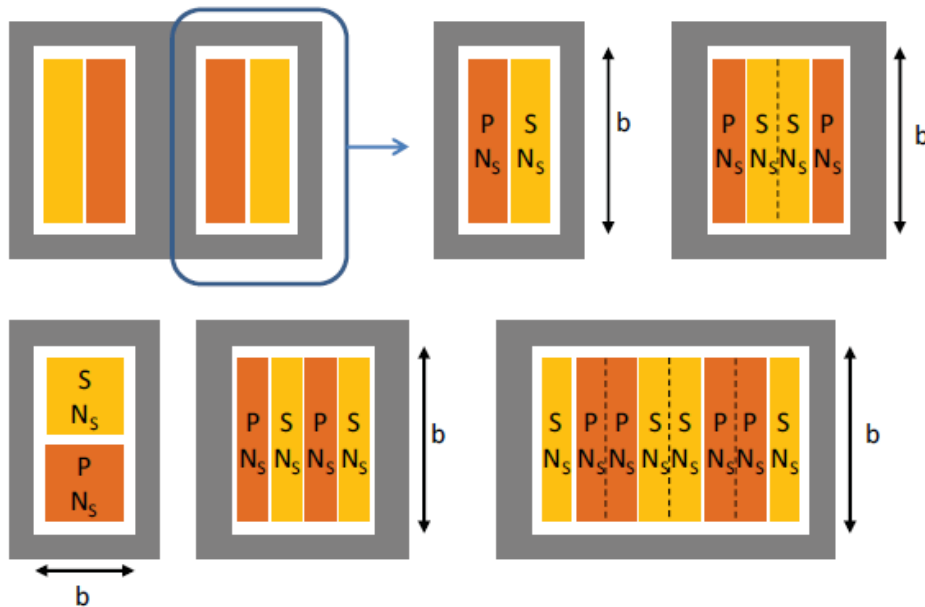


Figure 4.4: Examples of how the winding breadth b and the number of turns per section are defined for some common winding geometries. [19, 27]

3. Recommended number of strands:

The recommended number of strands required to attain the optimal coil design in order to reduce losses at high frequencies can be calculate from Eq (4.3) taking into account the strand diameter.

$$n_e = k \frac{\delta^2}{N_s} \quad (4.3)$$

Where k is a constant for the diameter of each strand of conductor which has been pre-calculated and can be obtained from Table 4.1 for each wire size and diameter. From the values of k in the table, k is measured in mm^{-3} . It is therefore required for b and δ to also be in mm so that the value of n_e will have no unit. The calculated value of n_e from Eq (4.3) is considered as a general indication and not a precise indication of the number of strands. Values of n within a tolerance range of $\pm 25\%$ is still acceptable and can be considered as a good choice.

Table 4.1: the parameters for economical Litz-wire designs [27]

Strand AWG size	32	33	34	35	36	37	38	39	40	41	42	43	44	45	46	47	48
Strand diameter (mm)	0.202	0.180	0.160	0.143	0.127	0.113	0.101	0.090	0.080	0.071	0.063	0.056	0.050	0.045	0.040	0.035	0.032
Economical F_R	1.06	1.07	1.09	1.11	1.13	1.15	1.18	1.22	1.25	1.30	1.35	1.41	1.47	1.54	1.60	1.64	1.68
k (mm^{-3})	130	203	318	496	771	1.2k	1.8k	2.8k	4.4k	6.7k	10k	16k	24k	36k	54k	79k	115k

4. Selection of final strand diameter and number:

In step 3, an array of similarly good design options considering different strand diameters is given. In order to select the best wire size, it is important to make sure that the design given by Eq. (4.3) fits the available window space. An approximation for this calculation can be made by assuming that total area of the actual copper can be achieved by the expression NnA_s , where the number of turns (N), the number of strands (n) and the cross sectional area of a single strand (A_s) are 25% - 30% less than the window area available for the winding. The largest number that fits the window can be considered if the recommended number of strands does not fit in the window. But if this requires more than 25% reduction in the recommended number of strands, one of the designs that fits could be used to achieve a similarly good performance at a much lower cost.

When the calculated n_e is chosen as the number of strands, there is corresponding AC resistance factor as shown in Table 4.1.

This information and a calculation of DC resistance makes it easy to put together a table of the AC resistance for the economical and effective design of each strand diameter thereby providing the possibility for trade-offs between cost and the losses. Given an AC resistance specification, it becomes possible to choose the lowest cost design that meets the required specification illustrated in the table [19,27,28]. Generally, higher operating frequencies requires a smaller nominal single wire diameter for optimum results [25].

4.2.2 Choosing construction

Simply twisting a large number of strands together instead of a constructed multiple level twisting (true Litz construction) could lead to a bundle level skin-effect problem where the high frequencies will discriminately flow on the surface strands leaving the inner strands less utilized. To avoid this problem, the maximum number of single strands that can be twisted together can be calculated from Eq. (4.4)

$$n_1 = 4 \frac{\delta^2}{d_s^2} \quad (4.4)$$

Where δ is the skin depth for a solid conductor given Eq (4.1) and d_s is the diameter of an individual strand.

If the total number of strands, n is less than $n_{1,max}$, then all the strands can be twisted together in one operation without encountering problems of bundle-level skin effect. If $n > n_{1,max}$, then it is recommended to utilize multiple twisting operations in order to improve performance. The first twisting step should combine $n_{1,max}$ or fewer strands. Further operations should only combine 3, 4, or 5 bundles from previous operations. [27][19][28]

4.3 Technical Basics and Calculation

4.3.1 Right-hand-rule

As current (I) flows through a conductor, a magnetic field (B) is created whose field lines are positioned concentrically around the conductor. Gripping a straight conductor in the right hand with the thumb running along the length of the conductor indicating the direction of flow of the current (I), then the fingers running along the circumference of the conductor indicates the direction of circulation of the magnetic field (B).

B also denotes the magnetic flux density which is proportional to the magnetic field intensity (H) and the magnetic permeability (μ) which is dependent on the type of material.

This relation can be mathematically represented as:

$$\begin{aligned} B &= \mu_0 * \mu_r * H \\ &= \mu * H \end{aligned} \tag{4.5}$$

Where:

μ_0 = the magnetic constant, permeability of free space ($4\pi * 10^{-7} \text{ N/A}^2$)

μ_r = the relative permeability.

4.3.2 How to calculate the number of turns in the primary coil

It depends on the magnetic induction you want your coil to work on. The equation below gives how to get the number of turns for the primary coil or transfer coil:

$$V = 4.44NBAf \tag{4.6}$$

Where N is the number of turns, B is the magnetic induction, A is the area of the core, and f is the frequency.

4.3.3 Skin-effect and skin depth

Current flowing through the conductor causes both internal and external concentric magnetic fields. This is illustrated by the magnetic field strength (H) as depicted in Figure 4.5. the magnetic field within the conductor itself creates a concentric and interfering eddy currents which impacts the current flow towards the outer layer with rising frequency (f). this effect causes the skin depth δ of the current to decrease. δ is the distance from the conductors surface, where the current density has dropped to $1/e$ (e = Euler's constant) of the amplitude value. This implies that, the measured ohmic resistance thus becomes frequency dependent and as such, its value rises as the frequency increases. Subsequently, conductor heating and other electrical losses arise due to increase in frequency. Moreover, HF-losses also takes place due to internal and external proximity effect.

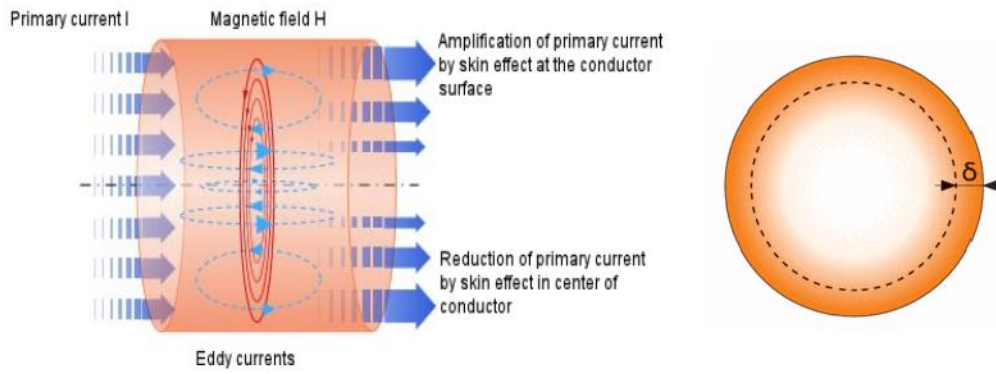


Figure 4.5: the magnetic field (H) and current flow in the inductor, and skin depth

The equation of skin depth is given in Eq (4.1) and it can also be re-written as $\delta = \frac{1}{\sqrt{\pi * \mu_0 * \sigma * f}}$.

Where:

μ_0 = the magnetic field constant (permeability of free space),

σ = conductivity of conductor material, and

f = frequency.

Table 4.2 provides information about some frequencies and their corresponding copper skin depth

Table 4.2: parameters for skin depth of copper Litz wire with frequency [25]

Frequency	δ (Copper)
10 kHz	0.66 mm
50 kHz	0.30 mm
100 kHz	0.21 mm
500 kHz	0.094 mm/94 μ m
1 MHz	0.066 mm
10 MHz	0.021 mm
100 MHz	0.0066 mm

4.3.4 Relationship of single wire diameter to range of frequency

In designing and constructing a high frequency litz wire and its resulting electrical performance, so many factors are put into consideration which are also its dependents. For every specific application, choosing the right single wire diameter is very paramount and some amount of experience is needed in choosing the optimum litz construction that can be economically and invariably manufactured because there are different design approaches that can give indistinguishable values of performance.

Table 4.3: the relationship between recommended single wire diameter and frequency range [25]

Range of frequency [kHz]		Nominal Diameter of single wire [mm]	
from	to	from	to
0.06	1	0.400	0.254
1	10	0.254	0.200
10	20	0.200	0.127
20	50	0.127	0.102
50	100	0.102	0.079
100	200	0.079	0.063
200	300	0.063	0.050
300	850	0.050	0.040
850	1400	0.040	0.030
1400	3000	0.030	0.020

Table 4.4: System specifications

Symbol	Meaning	Value
P_{out}	Rated Output Power	16.7 W
V_{out}	Output Voltage	11.1 V dc
f	Operating Frequency	50 kHz

Table 4.5: design parameters for the transmitting and receiving coils I designed

Parameters	Value
Nominal diameter of single wire \varnothing_{ED} (mm)	0.102
Total number of windings	30
Number of windings per layer	10
Number of winding layers	3
Ferrite sheets L*W*H (mm)	120x120x0.1
Dimension of ferrite core (mm)	36x22
Gap between the coils (mm)	Approx..11

I used ferrite cores and ferrite sheets for coupling enhancement, magnetic shielding, and EMI suppression. Apparently what I ordered online was not what I was expecting, my core dimensions should have been in centimetres but I could only see the materials in millimetres, so I had to improvise; instead of winding the litz-wire inside the ferrite core, I had to wind the wire around the core and it worked. The ferrite sheets are flexible and have a self-adhesive mounting tape which aided in winding the coils. I also used some double-sided adhesive tapes to hold down the wire for each layer. A figure of the transmitter and receiver coils I constructed is shown in Figure 4.6 below.

The voltage that is applied to the primary resonator which is produced by the full-bridge inverter, is in most cases a square wave. This square wave consists of high-order harmonics which is basically analysed in [24] with an example to it. The mathematical expression can be found in Eq (4.7) below.

$$V_{pk} = \left(\frac{4V_{dc}}{k\pi}\right) \sin\left(\frac{k\pi D}{2}\right) \sin\left(\frac{k\pi}{2}\right) \quad (4.7)$$

Where V_{pk} is the peak voltage of the k th harmonic of the square wave; V_{dc} is the DC input voltage of the inverter; D is the duty ratio of the inverter which can be regulated by using phase-shift control. By regulating the duty cycle ratio of the full-bridge inverter, the high-order harmonics in the square wave can be varied. In my project, a duty cycle of 0.75 is used for the first leg of the inverter and 0.25 for the second leg in the dSPACE control system.

Note that in simulations, core losses are neglected. And also, when you further reduce the gap between the coils, that does not mean the efficiency of the system will increase; simply because of the rising proximity effect [24].



Figure 4.6: the transmitter (Tx) and receiver (Rx) Litz-wire coil I constructed

5 CHALLENGES

Initially in my simulation, I was using a PWM before I finally switched to a pulse generator to drive my inverter and resonant circuit. At that stage there was a short circuit in the circuit because the bipolar switches in the inverter were switching ON at the same time. That is common in IGBT's because their switches close faster than they open. This switching problem was solved using a dead-time on-delay in the pulse-width modulator which gives an instruction to the set on switch to delay before it comes ON or OFF. There was also a voltage source ripple when I started my modelling because my plan was to supply the system with an AC voltage and then rectify to DC for the inverter, but this problem was solved by replacing the AC voltage source and rectifier with a 400V DC source, and that even made the whole circuit simpler and easy to implement.

Furthermore, due to the high resonating frequency and higher switching frequency, the switching pulses and the input/output waveforms from the transformer and to the load was too fast and close to each other that I had to zoom almost 400% to have a clear view of the waveforms. So, I reduced my step time to 0.0001 to capture a better sinusoidal waveform and back to 0.04 to get an overview of the entire waveform.

During my laboratory testing, there was no current flow at high frequency (2kHz and above) because a large capacitor ($8\mu F$) was used. This problem was solved by calculating and selecting the appropriate resonant capacitor for the system.

Finally, there is a lot of current spikes in the inverter during the laboratory tests. This could be due to EMI from other equipment in the laboratory and due to time constraints, I could not troubleshoot the cause of these current spikes.

6 RESULTS AND ANALYSIS

The wireless charger for small electric vessels is composed of the DC power source, full-bridge inverter and its driver, the LLC resonant tank, inductive coils, full-bridge rectifier and the DC load. The LLC resonant tank excited with an AC source from the full-bridge inverter is basically a collection of the series resonant capacitor C_r , series resonant inductor L_r , parallel magnetizing inductor L_m and an equivalent load resistor R_{eq} . In my simulation, I used MATLAB/SIMULINK software and for experimental verification, the Drives Board from University of Minnesota was used in designing the hardware which was controlled using dSPACE control system. The simulation circuit and hardware design are shown in Figure 6.1 and Figure 6.2 respectively. The simulation circuit in Figure 6.1 is also used to run tests for small application as described in the hardware.

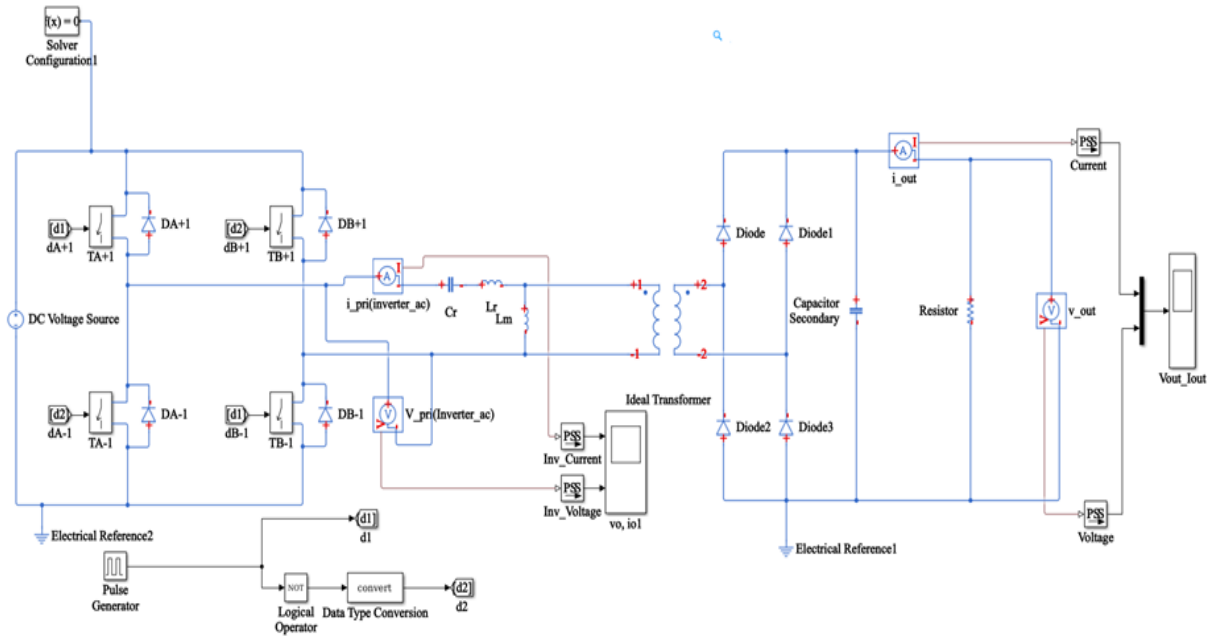


Figure 6.1: the simulation circuit for the wireless charger

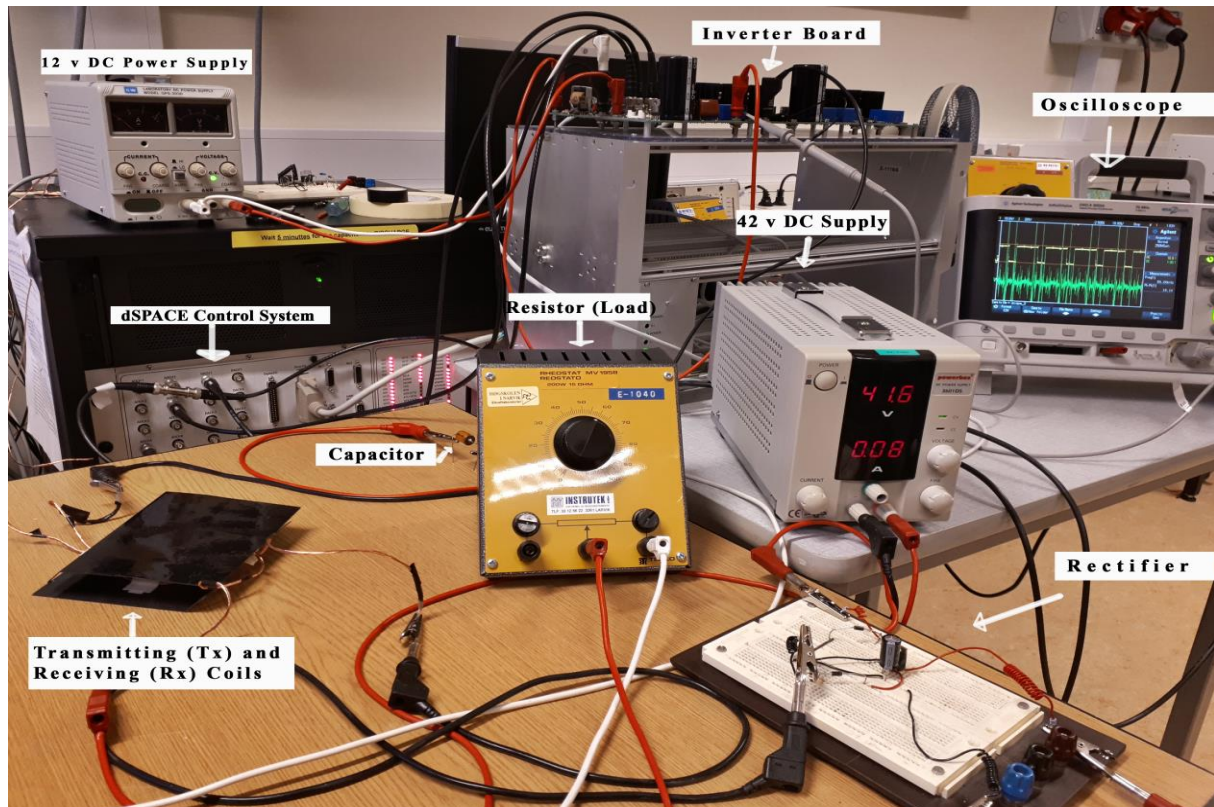


Figure 6.2: the hardware laboratory setup corresponding to the circuit above

The design is based on the application circuit in Figure 6.1 above, where individual resonant components are implemented. The target specifications are summarized in Table 6.1.

Table 6.1: the target specification for the resonant converter

Item	For Heavy Load	For Small Application
Input voltage, V_{in}	400V DC	12V DC
Output voltage and current V_o, I_o	600V DC, 1.7A	11.1V DC, 1.5A
Output power, P	1020W	16.7W
Efficiency, η	>98%	>98%
Resonant frequency, f_r	115kHz	50kHz
Frequency range	56.5kHz - 150kHz	24.5kHz - 74kHz
Resonant Inductor L_r	71.2uH	8.88uH

Resonant Capacitor C_r	0.027 μ F	1.14 μ F
Magnetizing inductance L_m	377.18 μ H	47.05 μ H
Resistor (Load)	128.423	6,975

Table 6.2: simulation and hardware results

Items	Simulation (400v)		Simulation (12v)		Lab Result	
	No Load	Full-Load	No Load	Full-Load	No Load	Full-Load
Voltage (v)	627	322	10.1	7.26	11.89	7.56
Current (A)	0	2.5	0	1.04	0	1.26

The simulated output voltage and current waveforms of the 400 v DC, and 12 v DC (hardware/small application) are shown in Figure 6.3 through Figure 6.9. While Figure 6.10 and Figure 6.11 are the laboratory measured results.

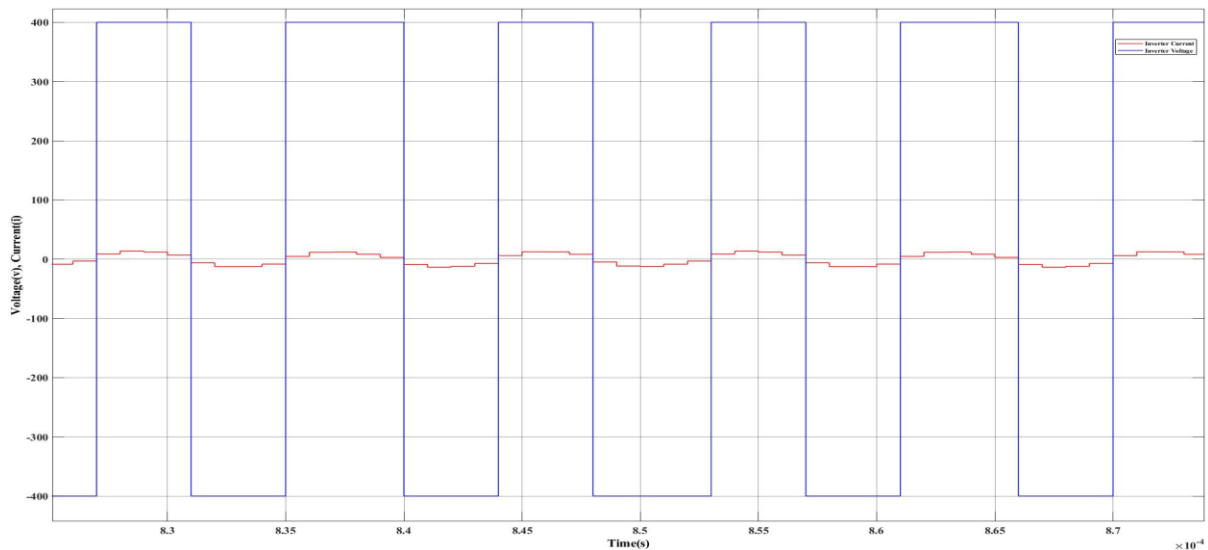


Figure 6.3: the 400vDC_Inverter Voltage and Current waveform at full load at 50% Duty Cycle

This is the expected waveform, as the converter is in steady state, the current and voltage repeats itself in an identical pattern.

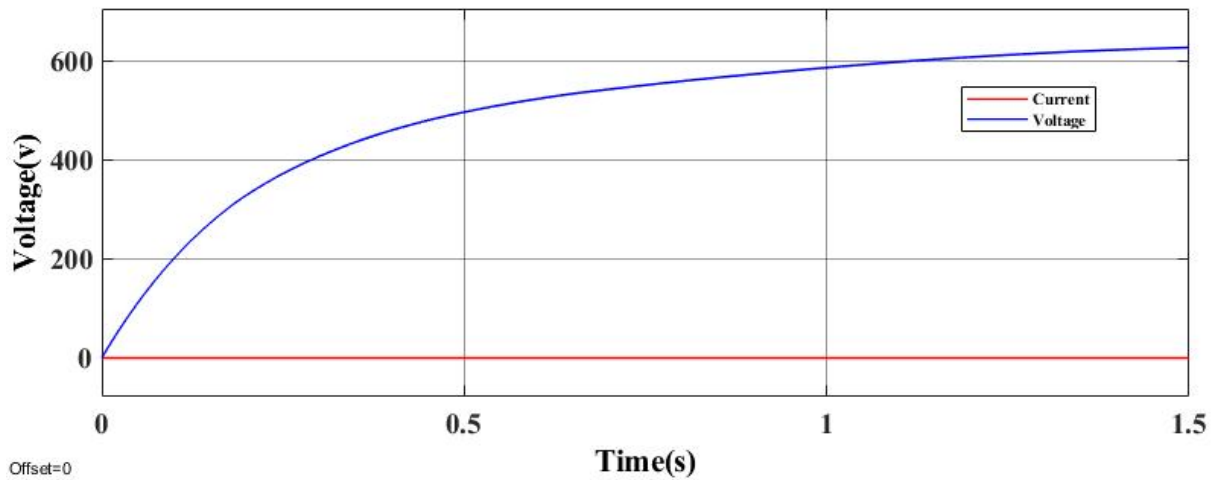


Figure 6.4: Output voltage of the 400 v DC source at no load is (627 V)

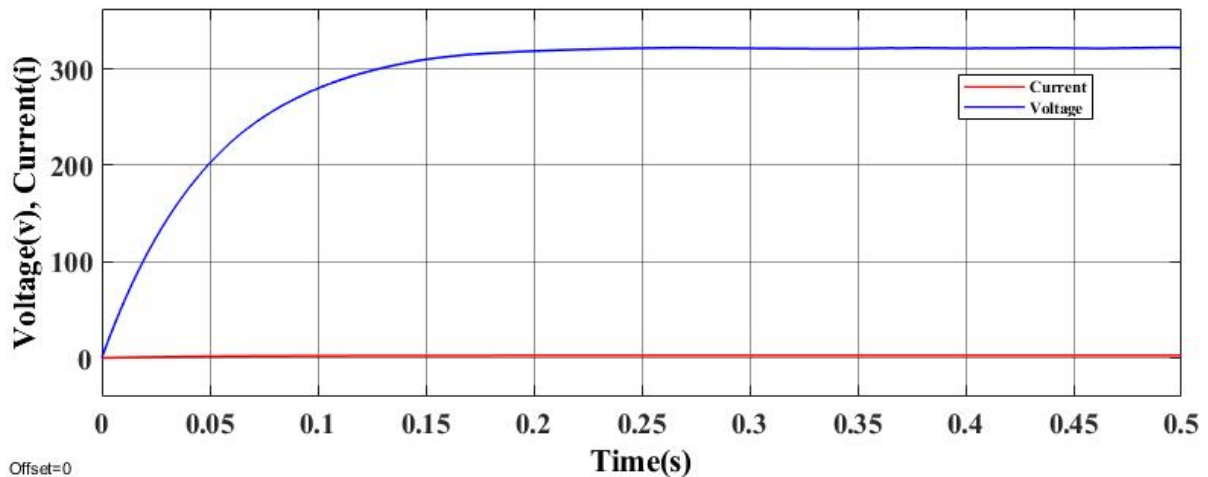


Figure 6.5: the waveform at full-load voltage (322 v DC) and current (2.5 A)

The target specification as shown in Table 6.1, I should have a 600 v DC output at no load but for some reason the systems keeps charging above 600 volts. So that is a good thing, the control should be put into consideration for future work.

The LLC tank circuit acts like a selective tuned circuit, i.e. it generates approximately a sine wave inverter output current and voltage waveform of switching frequency f_s . The converter in closed-loop and open loop are simulated by MATLAB/SIMULINK software. When the operating frequency is higher than the frequency at the peak voltage gain of the LLC resonant tank with different loading conditions, a ZVS condition is attained by the MOSFET when they are in their turn-on transition. To produce a ZVS condition, there should be an inductive impedance; so that the resonant current will lag supply voltage. The magnetizing inductor L_m

should have the ability to supply the needed quantity of inductive energy. The L_m value is carefully chosen in such a way that the magnetizing current would not be more than 20% of the resonant current. And at the same time, in order to reduce the losses gotten from conduction, the magnetizing inductor L_m value is meant to be high, but this same L_m value needs to be as small as possible to achieve a successful ZVS. [22]

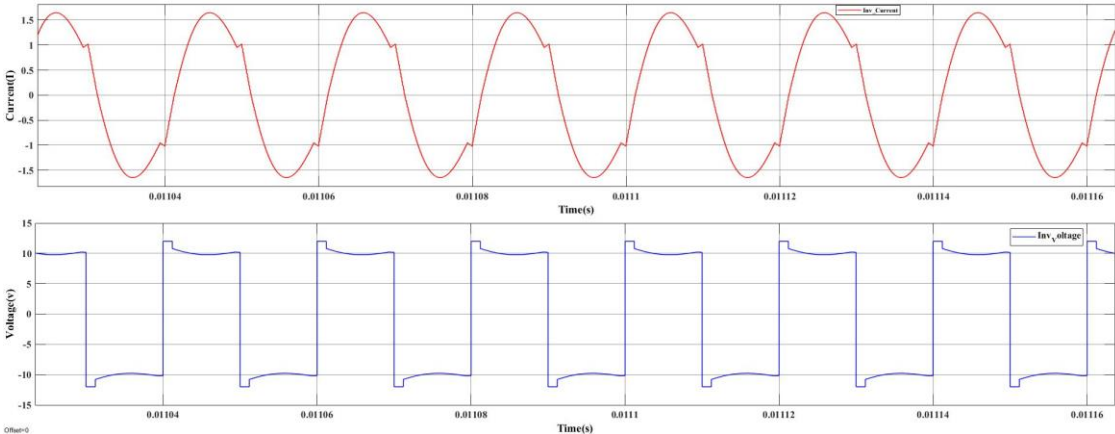


Figure 6.6: the 12v DC Inverter Voltage and Current waveform at full load (closed circuit) at 50% Duty Cycle

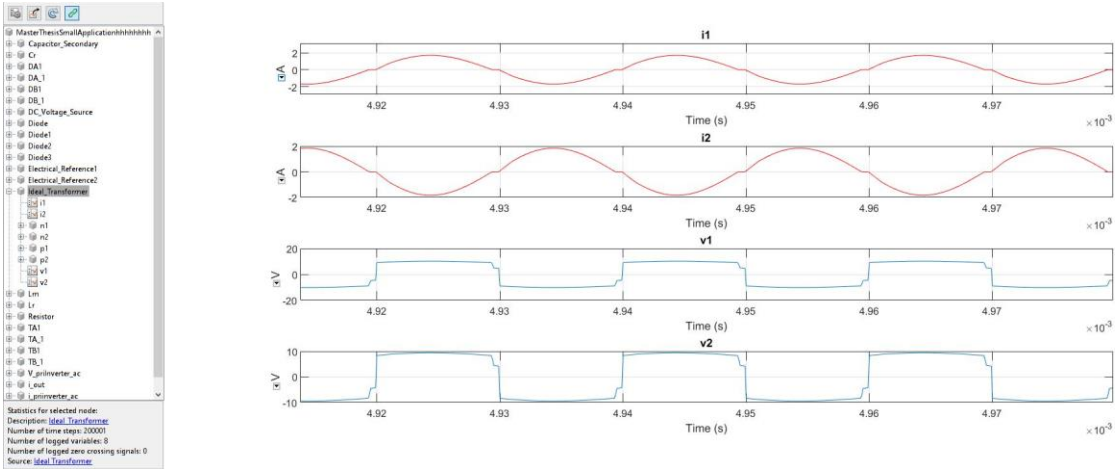


Figure 6.7: 12vDC_Transformer input and Output V&I waveform at full load (closed circuit) at 75% duty cycle

My converter’s operation is in steady-state because my current and voltage repeats itself in an identical pattern. From the figures above, the inductor voltage does begin and end at the exact same value of each period, and it continues to do so because the input voltage and duty cycle are kept constant.

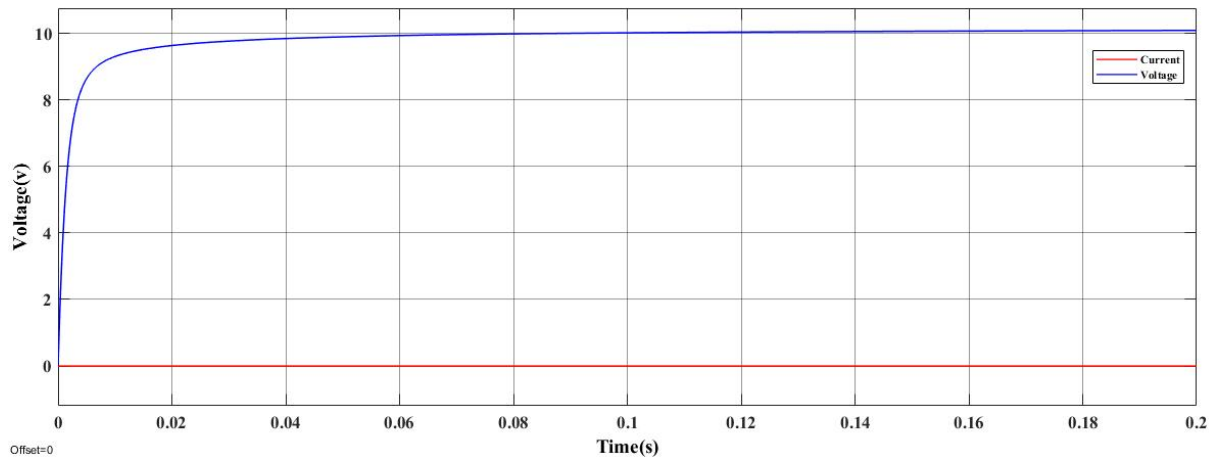


Figure 6.8: 12v DC Output Voltage at no load (open circuit) (10.1 V)

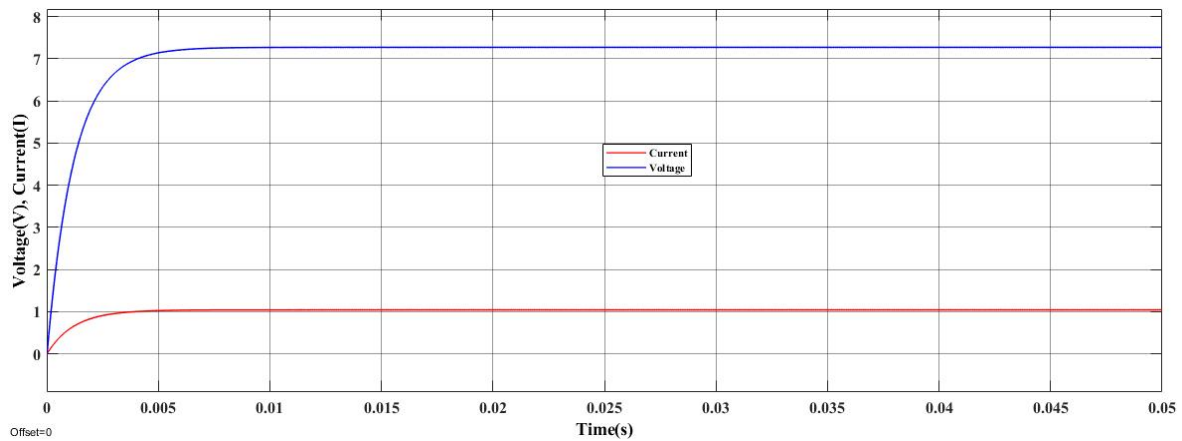


Figure 6.9: output waveform for 12 v DC at full-load (6.975 ohms), (7.26V), (1.04 A)

6.1 Hardware (Small Application)

I noticed that while testing, at low frequencies, there is a high pitching noise (i.e. the lower the frequency, the higher the pitching noise).

In order to reduce the rate of misalignment, the primary and secondary coils were placed right on each other and due to time constraint I was not able to carry out more tests like the farthest distance to which energy can be transferred from the primary coil to the secondary and at what efficiency. But I successfully transferred energy from the transmitter to the receiver at a measured distance of 1.6cm.

Figure 6.10 below shows the measured output voltage of the wireless charger using a multimeter and Figure 6.11 shows the measured output waveforms of the inverter when the

duty ratio is 1, compared with simulation results in Figure 6.6. The measurements agree well with the simulation results.

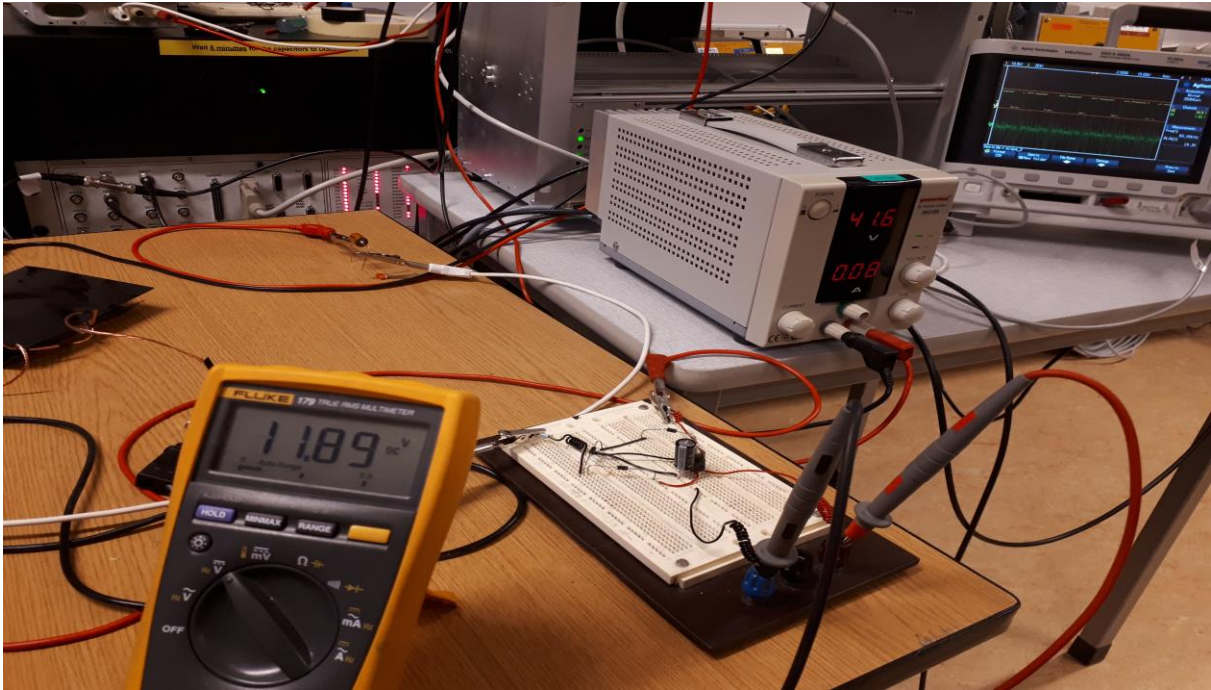


Figure 6.10: the output voltage of the laboratory setup

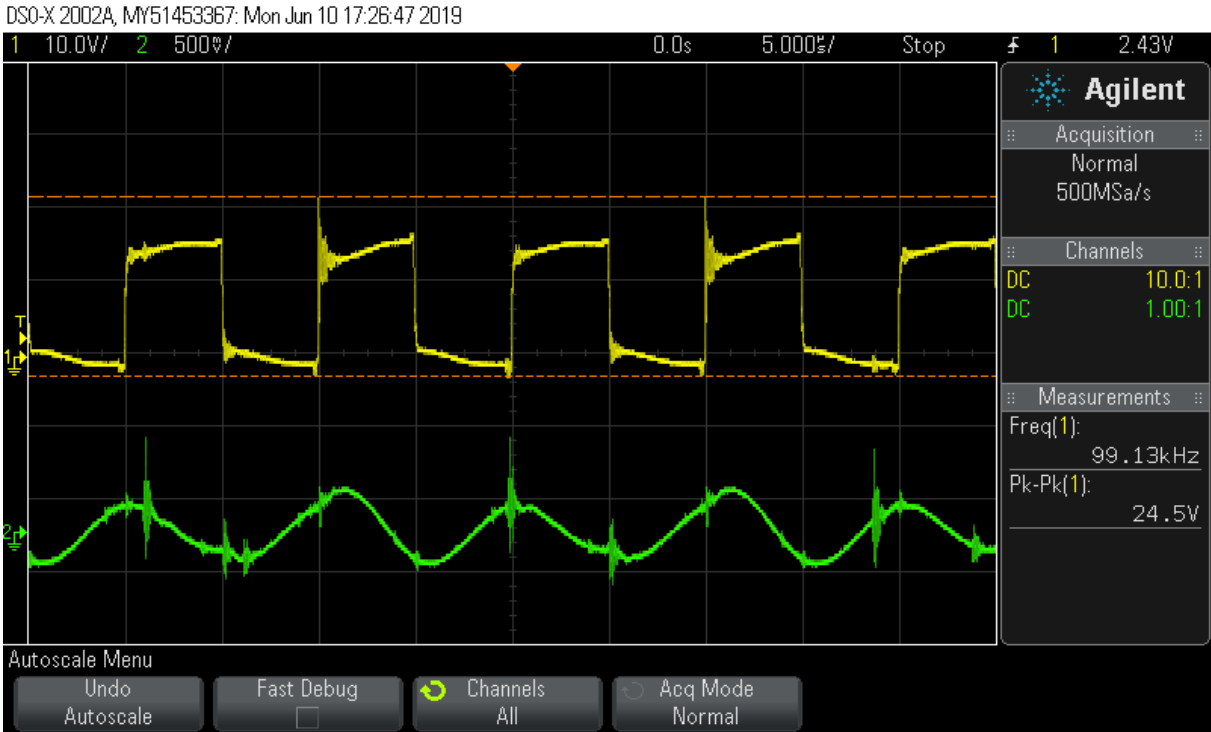


Figure 6.11: the waveforms of the output voltage and current of the inverter

7 CONCLUSION

A novel wireless charging system for Small Electric Vessel (GMV Zero) is proposed and successfully modelled, simulated, designed and constructed. All the project's objectives are met.

Both theoretical simulation and experimental investigations are executed to cross check the effectiveness of the design parameters for wireless charging system for small electric vessels in this research work. It is noticed that the MATLAB/SIMULINK simulation results agree well with the laboratory experimental results. The results are verified with a compact and efficient low cost 12/24 V prototype design. The efficiency of the power transfer is influenced by its operating frequency, coil arrangement and design, and physical air-gap between the primary and the secondary coils. The efficiency of the power transfer gets to its peak value only at the operating resonant frequency and it diminishes with the increase in spacing between the transmitting and receiving coils. The analysis of this project provides an authentic guideline to designing an efficient and cost-effective wireless charging system for small Electric Vessels.

7.1 Future works

- 1 The implementation of multiple coils to reduce misalignment as described in [15, 17].
- 2 The use of robot arm to automatically align the transmitting coil to the receiver to reduce the rate of misalignment as described in [24].
- 3 Introduction of a control algorithm to maintain the voltage when the load is getting near to being fully charged or when fully charged.

REFERENCE

- [1] G. Gildi, J. A. Suul, F. Jensen, and I. Sørfonn, “Wireless Charging for Ships, High-power inductive charging for battery electric and plug-in hybrid vessels,” *IEEE Electrification Magazine*, pp. 23 -32, Sept. 2017.
- [2] I. Nastali, “Electrified fishing in Norway,” <https://www.imarest.org/themarineprofessional/item/2498-electrified-fishing-in-norway>, *Institute of Marine Engineering, Science & Technology (IMAREST), The Marine Professional*, July. 2016; retrieved on 21st December 2018.
- [3] GMV, “Bnr. 138 – GMZ Zero,” <https://www.gmv.no/portfolio-item/bnr-138-gmv-zero/>, *GMV Grovfjord Mek. Verksted AS*, retrieved on 21st December, 2018.
- [4] Anish, “Battery Charging On Board Ship,” *Marine Insight*, <https://www.marineinsight.com/marine-electrical/battery-charging-on-board-ship/>, retrieved 8th November, 2018.
- [5] MOBIMAR (Mobile Marine Applications), “Electric Propulsion and Charging,” <http://www.mobimar.com/electric-propulsion-and-charging>, retrieved 13th November, 2018.
- [6] Z. Jianyun, C. Li, W. Bin, X. Linjuan, “Optimal design of a hybrid electric propulsive system for an anchor handling tug supply vessel,” *Applied Energy* 226 (2018), pp. 423-436, 2018.
- [7] M. Lempriere, “Wireless power transfer: working on the future of electric vehicles,” <https://www.power-technology.com/features/featurewireless-power-transfer-working-on-the-future-of-electric-vehicles-5933632/>, retrieved 2nd November, 2018.
- [8] G. Liu, and B. Zhang, “Dual-Coupled Robust Wireless Power Transfer Based on Parity-Time-symmetric Model,” *Chinese Journal of Electrical Engineering*, Vol.4, No.2, pp. 50-55, June 2018.
- [9] T. Q. Dinh, T. M.N. Bui, J. Marco, C. Watts, J. I. Yoon, “Optimal Energy Management for Hybrid Electric Dynamic Positioning Vessels,” *IFAC Papers Online*, pp. 98-103, 2018.
- [10] K. A. Kalwara, M. Aamir, and S. Mekhilef, “A design method for developing a high misalignment tolerant wireless charging system for electric vehicles, Measurement,” Vol 118, pp. 237-245, March 2018.
- [11] G. Liu, and B. Zhang, “Dual-Coupled Robust Wireless Power Transfer Based on Parity-

- Time-symmetric Model,” *Chinese Journal of Electrical Engineering*, Vol.4, No.2, pp.50-55, June 2018.
- [12] Y. Ra’di, B. Chowkwale, and C. Valagiannopoulos, “On-Site Wireless Power Generation,” *IEEE Transactions on Antennas and Propagation*, Vol. 66, No. 8, pp. 4260-4268, August 2018.
- [13] A. Namin, E. Chaidee, T. Sriprom, and P. Benchua, “Performance of Inductive Wireless Power Transfer between Using Pure Sine Wave and Square Wave Inverters,” *IEEE International Transportation Electrification Conference & EXPO Asia-Pacific*, 2018.
- [14] A. Ahmad, M. S. Alam “A Comprehensive Review of Wireless Charging Technologies for Electric Vehicles,” *IEEE Transactions on Transportation Electrification*, Vol. 4, No. 1, pp. 38-59, March 2018.
- [15] Fraunhofer IISB, “Inductive Charging System,” *Fraunhofer Institute for Integrated Systems and Device Technology*,
https://www.iisb.fraunhofer.de/content/dam/iisb2014/en/Documents/Research-Areas/vehicle_electronics/FraunhoferIISB_Brochure_VehicleElectronics_Inductive%20Charging.pdf, retrieved 22nd January 2019.
- [16] C. Joffe, S. Ditzte and A. Roßkopf, “A Novel Positioning Tolerant Inductive Power Transfer System,” *2013 3rd International Electric Drives Production Conference, IEEE Xplore*, pp. 1-7, October 2013.
- [17] C. Joffe, A. Roßkopf, S. Ehrlich, C. Dobmeier, M. Marz, “Design and Optimization of a Multi-Coil System for Inductive Charging with Small Air Gap,” *2016 IEEE Applied Power Electronics Conference and Exposition, IEEE Xplore*, pp. 1741-1747, March 2016.
- [18] J. O. Attia, “PSPICE and MATLAB for power electronics: An Integrated Approach,” *CRC Press Taylor & Francis Group*, Second Edition, pp. 222-230, ISBN: 978-1-4200-8658-4.
- [19] S. Pu, “Analysis, Design and Construction of an LLC Resonant Converter,” *Graduate Faculty of Auburn University, Alabama*, pp. 45-57, May 2016.
- [20] Alldatasheet.com, “High and Low Side Driver,” *IR2110 Datasheet(PDF) - International Rectifier*, <http://www.alldatasheet.com/datasheet-pdf/pdf/82793/IRF/IR2110.html>, Data Sheet No. PD60147, pp. 1-18, accessed 10th April, 2019.

- [21] Alldatasheet.com, “High Voltage MOS Gate Driver,” *IR2110 Datasheet(PDF) - International Rectifier*, <http://www.alldatasheet.com/datasheet-pdf/pdf/323402/IRF/IR2110.html>, Data Sheet No. PD-6.011B, pp. 1-24, accessed 10th April, 2019.
- [22] K. P. Panda, S. Rout, “A Cost-Effective Design and Analysis of Full bridge LLC Resonant Converter,” *International Journal of Energy and Power Engineering*, Vol. 10, No. 8, pp. 1143-1150, 2016.
- [23] S. K. Samal, D. P. Kar, P. K. Sahoo, S. Bhuyan, and S. N. Das, “Analysis of the Effect of Design Parameters on the Power Transfer Efficiency of Resonant Inductive Coupling based Wireless EV Charging System,” *International Conference on Innovations in Power and Advanced Computing Technologies, IEEE*, pp. 1-4, 2017.
- [24] W. Zhong and D. Xu, “Wireless EV charging system without Air-gap and Misalignment,” *IEEJ, The 2018 International Power Electronics Conference*, pp. 2569-2575, 2018.
- [25] Elektrisola Dr. G. Schildbach, “Elektrisola Litz Wire,” <https://www.elektrisola.com/en/home.html>, retrieved 6th May, 2019.
- [26] AET, “HF Litz Wire,” *AET_Specification and configuration of offered HF litz wires*, <https://en.aet.com.pl/HF-LITZ-WIRE/SPECIFICATION>, ISO 9001, 2015, retrieved 3rd May, 2019.
- [27] C. R. Sullivan, R. Y. Zhang, “Simplified Design Method for Litz Wire,” *IEEE*, pp. 2667-2674, 2014.
- [28] C. R. Sullivan, “Optimal Choice for Number of Strands in a Litz-Wire Transformer Winding,” *IEEE transactions on power electronics*, Vol. 14, No. 2, pp. 283-291, March 1999.
- [29] S. Abdel-Rahman, “Resonant LLC Converter: Operation and Design,” *Infineon design example-resonant LLC converter operation and design*, Vol 1.0, pp. 4-14, September 2012.
- [30] Alldatasheet.com, “3-Phase Bridge Driver,” *IR2133 Datasheet(PDF) - International Rectifier*, <http://www.alldatasheet.com/datasheet-pdf/pdf/84512/IRF/IR2133.html>, Data Sheet No. PD60107, pp. 1-8, April 2004. Accessed 13th May 2019.
- [31] S. Aldhafer, “Design and Optimization of Switched-Mode Circuits for Inductive Links,” *PhD Thesis, CRANFIELD University, Energy & Power Engineering Division*,

pp. 9-10, January 2014.

- [32] Circuits today, “Full Wave Rectifier-Bridge Rectifier-Circuit Diagram with Design & Theory,” Electronic Circuits and Diagrams-Electronic Projects and Design, August 2009. <http://www.circuitstoday.com/full-wave-bridge-rectifier>, retrieved 9th June 2019.